NEW INSIGHTS ON MINERALOGY AND GENESIS OF KAOLIN DEPOSITS: THE BURELA KAOLIN DEPOSIT (NORTHWESTERN SPAIN)

Emilio Galan[1], Patricia Aparicio[1], Juan Carlos Fernández-Caliani[2], Adolfo Miras[1], Marcial G. Márquez[1], Anthony E. Fallick[3], Norbert Clauer[4].

[1] Departamento Cristalografía, Mineralogía, y Química Agrícola, Facultad de Quimica, University of Sevilla, Spain

[2] Departamento de Geologia, Facultad de Ciencias Experimentales, University of Huelva, Spain[3] Scottish Universities Environmental Research Centre, East Kilbride, Glasgow G75 0QF, UK

[4] Laboratoire d'Hydrologie et de Géochimie de Strasbourg (CNRS-UdS), University of Strasbourg, France

CORRESPONDING AUTHOR: Patricia Aparicio **paparicio@us.es**

NEW INSIGHTS ON MINERALOGY AND GENESIS OF KAOLIN DEPOSITS: THE BURELA KAOLIN DEPOSIT (NORTHWESTERN SPAIN)

E. Galan[1], P. Aparicio[1], J.C. Fernández-Caliani[2], A. Miras[1], M.G. Márquez[1], A.E. Fallick[3], N. Clauer[4].

[1] Departamento Cristalografía, Mineralogía, y Química Agrícola, Facultad de Quimica, University of Sevilla, Spain

[2] Departamento de Geologia, Facultad de Ciencias Experimentales, University of Huelva, Spain[3] Scottish Universities Environmental Research Centre, East Kilbride, Glasgow G75 0QF, UK

[4] Laboratoire d'Hydrologie et de Géochimie de Strasbourg (CNRS-UdS), University of Strasbourg, France

ABSTRACT

The Burela deposit is the largest kaolin deposit in Spain, mined for more than 50 years, the product being mainly used for porcelain. Kaolin is dominantly associated ~~to~~ with Lower Cambrian felsites, interbedded with quartzites, micaschists and metapelites (Cándana Series), and was strongly folded during the Hercycian orogeny. Kaolin layers were ductile and incompetent materials among more competent ones, producing many slides with a diastrophic appearance. Consequently, kaolin outcrops are morphologically very variable, -i.e. pockets -, and interlayered between metapelites and/or quartzites, resulting in ~~difficult~~ complication for prospection and mining.

The kaolin consists mainly of kaolinite, tubular halloysite, and spherical allophane along with quartz and minor illite. The content of kaolin minerals reaches up to 90% in the finer fraction (<2μm and <1μm).

Geochemical analyses of trace and REE show a close relationship between kaolin and associated rocks. Two kaolin types can be differentiated: (i) massive, associated to felsite; and (ii) related to metapelite. A temperature range from 20 to 35°C, with an average of approximately 28ºC was calculated on the basis of the isotopic signatures ($\delta^{18}O$, δ D) for the kaolin materials. This scatter suggests that if continental weathering was involved in the kaolin formation on the lower side of the temperatures, it was not the only process, especially for kaolin associate ~~to~~ with felsites and metapelites. The higher temperatures are indicative of a hydrothermal auto-metamorphic alteration, followed by a folding of the series that induced an apparently chaotic kaolin distribution with a combined continental weathering superimposed on the previous low-temperature hydrothermal felsite transformation.

Key words: kaolin genesis, trace elements, isotopes, halloysite, Galicia, Spain

INTRODUCTION

The origin of primary kaolin deposits is usually a matter of controversy because kaolinite can be formed *in situ* by weathering reactions (supergene kaolins), hydrothermal alteration during the late stages of magma cooling (hydrothermal kaolins), or by a combination of both processes (Murray, 1988). Kaolinite can be formed also within sedimentary continental basins by diagenetic processes (Galán and Ferrell, 2013). Various criteria and indicators have been proposed to distinguish supergene from hypogene kaolins (e.g. Dill et al., 1997, Gilg et al., 1999), although some of them are considered as ambiguous. Unravelling the genesis of kaolinite in deeply weathered magmatic rocks is~~, therefore,~~ one of the most important challenges faced by clay geologists.

In the Variscan belt of Galicia (NW Spain) kaolinization of crystalline rocks is widespread. Large high-grade deposits of kaolin (e.g. Vimianzo, Nuevo Montecastelo) and other minor occurrences are found in association with weathered granites. The combined oxygen and hydrogen isotope composition of kaolinite from such deposits is consistent with data of supergene kaolin formation (Clauer et al., 2010, 2015; Fernández-Caliani et al., 2010~~; Clauer et al. submitted~~). However, some deposits associated with felsite dykes or sills and

quartz vein networks could have been formed *in situ* by complex fluid/rock hydrothermal and supergene interactions.

The Burela kaolin deposit (Northern Galicia) is a volcanic-hosted deposit, which is of particular interest in addressing the origin and timing of kaolinization. Volcanic-hosted kaolin occurrences of no current economic interest are also found in other areas of Spain, such as the Canary Islands and within the volcano-sedimentary complex of the Iberian Pyrite Belt., ~~but~~ However it is in the Burela area ~~that the type~~ where kaolinization is best represented. The deposit is geologically located (Fig. 1) in the West Asturian-Leonese Zone (WALZ), one of the major tectono-stratigraphic terranes into which the Iberian Massif is classically subdivided (Julivert et al., 1972). The WALZ exposes Precambrian to Devonian metasediments that experienced the effects of the Variscan orogeny between Late Devonian and Late Carboniferous times (Martínez-Catalán et al., 1997; Pérez-Estaún and Bea, 2004).

The main Burela quarries are ~~of~~ San Andrés and Ramón Fazouro that are located near the western edge of Fazouro village (Fig. 1). The kaolin is spatially and genetically related to felsites and a swarm of quartz-porphyry dykes that intruded Lower Cambrian metasediments. Kaolin is dominantly associated with Lower Cambrian felsites, interbedded with quartzites and sandstones, and metapelites (Cándana Series), and ~~it was~~ which were strongly folded during the Hercynian orogeny. Kaolin-rich layers ~~were~~ became a ductile and incompetent materials interleaved among the more competent ones, producing many slides with a diastrophic appearance. Consequently, the kaolin outcrops are morphologically very variable (i.e. pockets) interlayered between other rocks, resulting in difficult prospection and mining.

This world-class kaolin deposit has been mined by ECESA for more than half a century (1957-2014), with the kaolin being mainly used as raw material in the manufacture of high quality ceramics, especially porcelain-ware. The kaolin material consists of a mixture of kaolinite and halloysite with minor allophane (Galán et al., 2013). The origin of this important economic deposit is still an ongoing matter of debate. It is unclear if extensive kaolinization resulted from hydrothermal (by meteoric fluids) alteration of felsitic rocks, or if weathering affected material that was already subjected to a first stage of ~~auto-~~low grade

~~metamorphic alteration~~ metamorphism, or a combination of the two processes induced the deposit (Galán and Martín Vivaldi, 1972). The aim of this paper is to revisit the arguments first presented, (i.e. hydrothermal alteration by meteoric fluids) on the basis ~~of~~ on new insights from mineralogy, trace-element geochemistry and stable isotope data~~., and to contribute to~~ Such understanding will be helpful for future ~~the~~ exploration for new deposits in the region and to the rationalization of ~~their~~ mining operations.

SAMPLING AND ANALYTICAL METHODS

A representative sampling of the Burela kaolin deposit was undertaken in the Ramón Fazouro quarry (Fig. 2). A total of forteen samples of ~~The~~ different kaolin occurrences and their associated rocks were sampled. Three size fractions (<45, <2 and <1 μm) were extracted from each whole rock by wet sieving, sedimentation in distilled water and centrifugation. The size fractions were mineralogically analysed by X-ray diffraction (XRD) on a Bruker D8 Advance instrument with a scanning speed of 0.5º(2θ)/min, 0.15 step/size, and Cu-kα radiation (40 kV, 30 mA). The quantitative composition was carried out following the procedures of Schultz (1964), Martín-Pozas et al. (1971) and Galán and Martín Vivaldi (1973) for the whole kaolin and the <45 and <2μm fractions. In order to resolve the unequivocal identification of kaolinite and halloysite from the XRD patterns, and to provide a method of quantification in these types of samples, a fitting process was applied to the 002 XRD reflections (~3.5 Å), using a pseudovoight function for minimising the effect of the Lorentz-Polarization factor, since this signal appears at relatively high angles (24-26º) (Márquez et al, 2009).

The Rietveld method was used with the TOPAS program to evaluate the mineralogical composition of the <1μm separates, to obtain a very precise mineralogical composition for this size fraction, potentially the least modified by contaminant minerals, and to quantify the proportions of the different kaolin minerals (e.g. kaolinite vs. halloysite). This procedure was applied to the <1μm fraction to relate the isotopic with the mineralogical data.

A few samples (5) were selected for high-resolution observation by a scanning electron (HRSEM) HITACHI S5200 instrument, fitted with an EDS detector. The particle morphology was also studied by atomic force microscopy with a Pico Plus instrument. In addition the country rocks were optically examined under polarizing photomicroscope. X-ray analyses and microscopy observations were performed at the CITIUS (Research Facilities Centre at the University of Seville, Spain).

For the bulk sample and <45 and <2 μm fractions, chemical analyses were carried out at the Activation Laboratories Ltd. (Ontario, Canada) following a lithium metaborate/tetraborate fusion technique that ensures dissolution of the entire sample. Major-element concentrations were determined by inductively coupled plasma-optical emission spectrometry (ICP-OES) on a Thermo Jarrell Ash ENVIRO II, and trace elements were analyzed by inductively coupled plasma-mass spectrometry (ICP-MS) on a Perkin Elmer Optima 3000. Quality control included the use of several certified reference materials, duplicates and blanks by the laboratory to check accuracy and precision. The chemical results were statistically treated in order to realize cluster analysis.

The mineralogical maturity of weathering was estimated using the mineralogical index alteration (MIA; Johnsson, 1993; Nesbitt et al., 1996), which is a dimensionless number between 0 and 100, calculated from mineral weight percentages derived from XRD analysis as follows:

$$MIA = [quartz / (quartz + K\text{-feldspar} + plagioclase)] \times 100$$

The chemical index of alteration (CIA, Nesbitt and Young, 1982) was calculated to evaluate the degree of chemical weathering. CIA is also a dimensionless number between 0 and 100, and shows the weathering of feldspar minerals. It is calculated using molecular proportions as follows:

$$CIA = [Al_2O_3/(Al_2O_3+CaO^*+Na_2O+K_2O)] \times 100$$

where CaO* presents the amount of CaO combined in the silicate fraction of the rock.

The stable isotope data were obtained in two different laboratories. In both places, samples were vacuum-degassed at 200ºC overnight to remove the interlayer and absorbed surface water prior to hydrogen isotope analysis. Then,

they were transferred to an out-gassed Pt crucible and the water released by heating was reacted with hot metal, producing H_2 for determination of δD. For the samples analysed at the Activation Laboratories (Canada), uranium at 900°C was used for D/H; for $\delta^{18}O$ analysis, BrF_5 at 650°C was reacted with the kaolin in a Ni chamber (Clayton and Mayeda, 1963) to generate O_2 that was reduced to CO_2 with graphite using Pt as catalyst at 550-600ºC. The precision at 1σ was ± 2‰ and 0.3‰ respectively for δD and δ18O. For those results obtained at East Kilbride (UK), dehydroxylation was achieved by heating the Pt crucible at 1200ºC by radiofrequency induction. The water released was converted to H_2 by reacting with Cr at 800ºC (Bigeleisen et al., 1952; Donnelly et al., 2001) in a multiple-pass system. The H_2 yield was measured manometrically and the δD determined on a gas-source mass spectrometer calibrated via water and mineral standards. Using these techniques, the NBS30 biotite standard gave a δD of -65‰ (V-SMOW) with an analytical reproducibility of ± 2‰ (1σ), ± 3‰ (1σ) being more appropriate for clay material. The oxygen isotope composition was determined by laser fluorination (Macaulay et al., 2000) using the Borthwick and Harmon (1982) ClF_3 modification of Clayton and Mayeda (1963). The precision for the clay material is ± 0.3‰ (1σ), the NBS28 quartz standard giving a $\delta^{18}O$ of 9.6‰ (V-SMOW). All clay isotope data are reported in parts per mil (‰) relative to the V-SMOW standard. No significant systematic isotope ratio difference between the two laboratories was observed. Stable isotopes were determined for four samples <45 μm fraction and eight samples <2 and <1μm fractions.

RESULTS AND DISCUSSION

Precursor host rocks

The Burela kaolin deposit is hosted in felsic porphyritic volcanic rocks interbedded with metasedimentary rocks, notably Lower Cambrian metapelites and quartzites (Cándana Quartzite). Representative mineralogical and chemical analyses of the precursor rocks of the kaolin deposit are given in Tables 1 and 2.

In thin section the felsic volcanic rocks display a holocrystalline, porphyritic texture (Fig. 3a), with phenocrysts of feldspar and patially reabsorbed quartz and set in a groundmass composed of fine-grained plagioclase, muscovite, and biotite (often altered to chlorite and associated to iron oxides). Quantitative XRD mineralogical determination showed that quartz accounts for 24-33% of the bulk sample, the feldspars range from 60 to 67%, with mica contents up to 30%. In partially altered samples, the amount of feldspars decreases by up to 35% yielding MIA values of 46. ~~Based on their total alkali-silica content ("TAS diagram", Le Bas et al., 1986),~~ According to the TAS binary diagram (total silica **vs** alkali content) of Le Bas et al. (1986), the felsic rocks can be classified as lavas of rhyolite-to-trachydacite composition.

The pelitic schists have a lepidoblastic texture and exhibit a strong penetrative foliation defined by preferred orientation of muscovite laths and quartz ribbons (Fig. 3b). ~~Hysterogenic~~ Chlorite and relict detrital grains of tourmaline, rutile and zircon are present as accessory phases. Intensely altered metapelitic rocks (MIA value as high as 87) are characterized by high content of clay minerals, notably kaolinite, ~~accounting~~ which can account for up to 38% (Table 1).

The Cándana quartzite shows a medium-grained granoblastic texture, in which quartz exhibiting undulate extinction typically forms a mosaic of polygonal crystals (Fig. 3c), with muscovite, tourmaline, zircon and rutile as subordinate minerals].

Mineralogical characteristics of kaolin.

The mineralogy of the bulk samples is dominated by highly variable contents of kaolin minerals (17-74%) and quartz (16-69%), accompanied by mica (up to 33%) (Table 3). Other phases that may be present, usually in subordinate or trace amounts, are feldspars and smectites. Additionally, SEM-BSE observations in combination with EDS microanalysis revealed a distinctive suite of heavy minerals including zircon, monazite, rutile, ilmenite and iron oxides.

~~For~~Within the <45μm fraction, the amounts of kaolin minerals ~~scatter notably in a~~ is variable with a wide concentration range (62-90%), with kaolinite being

dominant over halloysite. The contents of quartz and illite were lower than 24% in all the samples, whereas feldspars, smectites and allophane were found as accessory phases. In the fine fractions, the amount of kaolin minerals reached up to 92 % (Table 4 ~~2~~). Traces of allophone~~, gibbsite~~ and chlorite were detected in some samples and fractions. The fractions <2µm and <1µm contains mostly kaolinite and halloysite, with minor illite and quartz (Table 4).

Tubular halloysite accounts for 11 to 60% of the kaolin, while kaolinite content varies between 23 and 60%, with kaolinite/halloysite ratios ranging from 6 to 0.5. These results substantially agree with the microscopic observations (Figure 4). Tubular crystals of halloysite (0.5-8µm of length) appear to be joined to book-like kaolinite aggregates (Figure 4a, 4e and 4f) and kaolinite crystals are oriented face to face (Fig 4 b and 4d). Halloysite crystals appear also in the form of clusters (Fig 4c). Spherical shaped particles (0.5µm in diameter) were also detected by AFM, which correspond to allophane: it is not common to find at the same time tubular and spherical halloysite (Fig 4f). Tubular halloysite mostly corresponds to a weathering phase while spherical halloysite is instead formed by direct precipitation (neoformation) and it is usually considered as a precursor of tubular halloysite (Duzgoren-Aydin et al. 2002).

Major and trace element geochemistry

Chemical ~~analysis~~ analyses of the whole rock samples shows that the geochemistry of major elements (Table 3) is largely dominated by Si and Al, reflecting the high content of kaolin minerals in the altered rocks. Silica displays a broad range of concentrations (58.2-76.3 wt % SiO_2), except for the altered quartzite (RF-12)~~. It~~ which is also strongly and negatively correlated with both the alumina content (r= -0.99) and the weight loss on ignition (LOI; r= -0.88). The highest abundances of alumina (23-27 wt % Al_2O_3) and LOI (8-12 wt %) were found in samples from the upper part of the studied section.

The remaining major elements, except potassium, are all present at concentrations less than 1wt%. The K_2O content varies from 4.8wt% to 0.8wt%, with a mean value of 2.3wt%. The variations are closely related to the presence

of orthoclase and muscovite in the samples. The low content of calcium and sodium oxides is ~~likely~~ considered due to weathering of the plagioclases. The CIA varies from about 65 in the fresh felsitic rocks to around 96 in the most weathered felsite, suggesting a significant removal of labile basic cations (mainly K, Na, and Mg) relative to stable residual elements (Si, Al, Fe). The loss of alkaline and alkaline-earth elements can be attributed to the alteration (kaolinization) of ~~alkaline~~ alkali feldspar and mica, which are the minerals in the felsitic rocks most prone to weathering. In addition, the CIA of the metapelite is 84%, which indicates that this rock is highly altered, as confirmed by the high kaolin minerals content (31wt%).

The fine-grained kaolin rich samples (the <45 and <2μm fractions) contain a higher proportion of alumina (up to 37 wt % Al_2O_3) and concomitantly less silica (44-59 wt %) (Table 5). An enrichment in titanium oxide is detected in metapelite (RF-2) and in the samples RF3-05, RF-12 and RF-14, when the major elements composition is normalized to felsite (RF-8) (Figure 5a). As was noted above, the metapelite presents abundant rutile. The other kaolin samples do not ~~present~~ contains any significant anomaly in comparison with the felsite host rock.

When the major element compositions of samples RF3-05, RF-12 and RF-14 are normalized to the metapelite reference (Figure 5b), no striking anomaly is visible and the signatures of the samples are very similar to metapelite. The ~~egregious~~ unexpectedly high anomaly is of 2.5 in the case of iron oxide for <45μm fraction of sample RF-14.

An enrichment in the high field strength elements (HFSE) Sc, Zr, Hf and Th has been detected in kaolin when the data are normalized to felsite (RF-8) (Figure 6a), probably due to their resistance to weathering (e.g. Middelburg et al., 1988; Panahi et al., 2000). Thus the HFSE remained relatively immobile, linked to resistant heavy minerals (zircon, monazite and titanium oxides) that tend to be residually concentrated in the finer fractions of the kaolin. A very high statistical correlation (r= 0.97) was obtained between Zr and Hf, so that both elements mostly reside in the crystal structure of zircon. Elevated correlation coefficients were also observed between Nb and Ta (r= 0.88) because of the close geochemical affinity of such elements. Thorium shows a positive correlation (r= 0.65) with the light rare earth elements (LREE) consistently indicating that it is

hosted by monazite, which is the only LREE-rich accessory phase occurring in the kaolin.

High enrichments for large ion lithophile elements (LILE), such as Rb, Sr and Cs, are found in relation to metapelite for the samples RF-12 and RF-14, especially in the <45μm fraction (Figure 6b). But, when the trace-element compositions of samples RF-3-05, RF-12 and RF-14 are normalized to the metapelite composition, no anomaly is apparent with the signature of these samples very similar to that of the metapelite. On the contrary, the major anomalies are for Cs, Tl, Pb, Rb, Sr and Ta of the felsite and the other kaolin samples. The LILE probably were preferentially removed from the felsite rock during kaolinization, as noted by the depletion of Rb, Sr, and particularly Ba, in the kaolin.

The kaolin is not especially enriched in trace elements, although the overall abundance varies with the grain-size distribution (Tables 6 and 7). The <45μm fraction of the kaolin tends to have greater concentrations (ΣREE= 237-440 ppm) than the whole sample (ΣREE= 65-209 ppm), indicating a relative accumulation of REE-carrying minerals in the finer fractions. Seemingly, kaolinite could have played a role in scavenging REE, as reported in some weathering systems (Putter et al., 2002; Papoulis et al., 2004). Exceptionally, the sample RF-17 is markedly depleted in total REE (whole sample: 29 ppm; <45μm fraction: 37 ppm; <2μm fraction: 85 ppm) relative to the felsite rock, although the REE concentration level also exhibits the same dependence on the particle size of the kaolin.

Similar overall enrichments in REE have been documented in weathering profiles developed on granitoids elsewhere in the Galician region (Galán et al., 2007, Fernández-Caliani et al., 2010). However, at the Burela deposit the total REE content shows no significant correlation with the intensity of the chemical alteration (as shown by the CIA values), suggesting that other processes of remobilization and redistribution of REE occurred in this deposit. In addition, all the samples yield a similar pattern of the REE composition: in fact the shape of the REE patterns is identical for all grain-size fractions, characterized by a slight LREE enrichment (La_n/Sm_n=3.50-13.56) and a HREE depletion (Gd_n/Yb_n= 1.70-5.24). The positive Ce anomaly is due to the residual character of this element, which undergoes only partial oxidation (Gouveia et al., 1993).

The REE diagrams of the kaolin whole samples normalized against the fresh felsite (Fig. 7a) exhibit a nearly flat pattern with a slight enrichment in heavy REE (HREE), which is more prominent in the fine-grained samples (Fig. 7b). The HREE distribution seems to be controlled, therefore, by HREE-enriched phases like zircon, ilmenite, and rutile (Laveuf and Cornu, 2009). These resistant minerals are not expected to be highly mobilized during alteration, and therefore they tend to be residually accumulated in the kaolin deposit, thus increasing the HREE budget. A cluster analysis identifies two types of geochemical signature (trace elements and REE) and the massive kaolin samples can be grouped into two main groups: associated to felsite and associated to metapelite (Figure 8).

In summary, the geochemical study of trace elements and REE showed a close relationship between kaolin and associated rocks, and from the geochemical point of view two kaolin types can be differentiated: massive kaolin associated to felsite and massive kaolin associated to metapelite, as above it has been largely discussed.

Stable isotope geochemistry

Combined stable oxygen and hydrogen (deuterium) isotope studies are commonly used to help discriminate between supergene and hypogene kaolins, and are considered to be the most powerful method to constrain temperatures of kaolinization (Gilg, et al. 1999).

The isotopic composition of nearly pure kaolin samples (<1μm fraction) from Burela deposit showed a narrow range of $\delta^{18}O$ values (19.8-21.0‰) and δD ratios ranging from -85 to -63‰, with the mean $\delta^{18}O$ and δD values being 20.4±0.4‰ and -74±3‰, respectively (Table 8). The scatter is close to the analytical error, indicating little geological variation. There is no statistically significant correlation between the two isotope ratios (r = -0.39, less than 80% significant for n=7). The mean water content of 7.4±0.4wt.% corresponds to 13.3±0.7 μmoles mg^{-1} of water, compared to the theoretical value of 14 for stoichiometric kaolin.

When plotted on a $\delta^{18}O$- δD diagram (Fig.9), all the points plot in the supergene field, *i.e.* on the right of the supergene-hypogene line of Sheppard et al. (1969), and very close to the kaolinite weathering line (KWL), which represents the isotopic compositions of kaolinites in equilibrium with meteoric waters at 20 °C. Similar values are given in the literature for residual kaolin deposits derived from Variscan granites (Bobos and Gomes, 1998; Boulvais et al., 2000; Clauer et al., 2010, 2015; Fernández-Caliani et al., 2010; Galán et al., 2010~~; Clauer et al., submitted~~). Here, the overall range of the calculated temperatures from studied kaolin separates ranges from 20 to 35 °C. These temperatures are compatible with a low-temperature hydrothermal activity, i.e.: a hydrothermal auto-metamorphic alteration that could occur on the felsite during submarine volcanic activity.

On the basis of a variety of assumptions involving plausible formation in an open system with high water–rock ratio and near-surface temperatures, a comparison with Delgado and Reyes (1996) modelling appears appropriate at this point, remembering that these authors assume an interaction with meteoric waters. Thus, the temperature and isotopic composition of the water from which kaolinite formed in equilibrium can be determined from the following equations:

[1] The meteoric-water equation: $\delta D = 8\delta^{18}O + 10$ (Craig, 1961)

[2] The equilibrium hydrogen isotope fractionation factor (α^H) between kaolinite and water (Gilg and Sheppard, 1996): $1000 \ln \alpha^{H}_{\text{kaol-water}} = -2.2 \times 10^6 \, T^{-2} - 7.7$

[3] The equilibrium oxygen isotope fractionation factor (α^{18}) between kaolinite and water (Sheppard and Gilg, 1996): $1000 \ln \alpha^{18}_{\text{kaol-water}} = 2.76 \times 106 \, T^{-2} - 6.75$.

In combining the equations of Sheppard and Gilg (1996) for kaolinite, $\delta^{18}O_w$, δD_w can be eliminated by using the meteoric water line equation, giving:

$$3.04 \, 10^6 \, T^{-2} = \delta^{18}O_k - 0.125 \, \delta D_k + 7.04$$

The crystallization temperature of kaolinite obtained by applying this equation to

the average of the measured <1 μm kaolin separates at 14.7 ºC is compatible with the supergene environment. This value is slightly higher than the current annual mean temperature of the Galician region (12 °C), but is a reasonable surface temperature expected during the Pliocene (Boulvais et al., 2000), with an accuracy of the equations representing the temperature dependence of the stable isotope fractionation equations (in (2) and (3) above) not at all well quantified. The possible mean isotopic composition of the meteoric water with which kaolinite crystallized at isotopic equilibrium has been calculated at $\delta^{18}O$ = -6‰ and δD = -40‰ (Fig. 9; mean values for the minerals taken from Table 8), using the above average temperature and the isotope fractionation factors of Sheppard and Gilg (1996) and Gilg and Sheppard (1996), respectively.

CONCLUSIONS

The Burela deposit is characterized by a high concentration of kaolin minerals (kaolinite and halloysite). In the coarse fraction the most abundant kaolin mineral is kaolinite of perfect pseudo-hexagonal morphology. Tubular halloysite is concentrated in the finer fractions.

The geochemical study of the trace elements and REE showed a close relationship between kaolin and associated rocks, and from the geochemical point of view two kaolin types can be differentiated: associated to felsite and associated to metapelite.

A felsite hydrothermal auto-metamorphic alteration is suggested for the origin of the kaolin, as an initial kaolinization step. Later a folding of the series led to an apparently chaotic kaolin distribution and a weathering action on the felsite completed the kaolin formation, superimposed on a low-temperature hydrothermal felsite transformation~~, as kaolinite is not mixed with common minerals typical for hydrothermal kaolins (pyrophyllite, dickite and nacrite, among others)~~. On the contrary, the occurrence of ~~gibbsite and~~ allophone in some samples point toward a supergene origin of the kaolin. On the other hand, micaschists were also kaolinized by weathering. The kaolin was a plastic incompetent material during the folding, which accumulated in the weaker zones,

and was a detachment level for the more competent materials (mainly quartzite and sandstone).

The isotopic composition of the nearly pure kaolin is consistent with a supergene origin. The mean $\delta^{18}O$ and δD values of the <1 μm fraction indicate that the most likely scenario is formation in equilibrium with meteoric waters at near surface temperatures (between 20 and 36°C). The scenario of a continental weathering followed by a low-temperature hydrothermal episode is therefore plausible.

These new insights into the genesis of the Burela volcanic-hosted kaolin deposit may provide useful information to guide kaolin regional exploration.

ACKNOWLEDGEMENTS

This work has been partially supported by the Spanish Ministry of Education and Science (Project BET2001-2415) and the Government of Andalusia through the Research Group Applied Mineralogy (RNM135). Authors are indebted to Dr. Collin Harvey and an anonymous reviewer for constructive and improving comments. Authors are grateful to Haydn H. Murray for his advice and kind collaboration during the field research (Figure 10).

REFERENCES

Bigeleisen, J., Perlman, M.L., Prosser, H.C., 1952. Conversion of hydrogenic materials to hydrogen for isotopic analysis. Anal. Chem. 24, 356-1357.

Bobos, I., Gomes, C., 1998. Greisen and post-greisen alteration of the Sao Vicente de Pereira kaolinite deposit, Portugal. Can Mineral, 36, 1615-1624.

Borthwick, J., Harmon, R.S., 1982. A note regarding ClF_3 as an alternative to BrF_5 for oxygen isotope analysis. Geochim. Cosmochim. Acta 46, 1665-1668.

Boulvais, P., Vallet, J.M.,, Estéoule-Choux,J., Fourcade, S., Martineau, F., 2000. Origin of kaolinization in Brittany (NW France) with emphasis on deposits over granite: stable isotopes (O, H) constraints. Chem. Geol. 168, 211–223

Clauer, N., Fallick, A.E., Galán, E., Aparicio, P., Miras, A., Fernandez-Caliani J.C., Aubert A. 2015. Stable isotope constraints on the origin of kaolin deposits from Variscan granitoids of Galicia (NW Spain). Chem Geol., 417, 90-101.

Clauer, N., Galán, E., Fallick, A.E., Fernández Caliani, J.C., Aparicio, P., Márquez, M.G, Miras A. 2010. Stable isotope constraints on the origin of kaolin deposits from variscan granitoids and felsites, and from sedimentary basins of galicia (NW Spain).Pp 97-98 in M.C. Hermosin, R. Celis, F. Bruna and P. Aparicio (editors) 2010 SEA-CSSJ-CMS Trilateral Meeting Books of Abstract of General Meeting.

Clayton, R.N., Mayeda, T.K., 1963. The use of bromine pentafluoride in the extraction of oxygen in silicates for isotopic analysis. Geochim. Cosmochim. Acta 27, 43-52.

Craig, H., 1961. Isotopic variations in meteoric waters. Science 133, 1702–1703.

Delgado, A., Reyes, E., 1996. Oxygen and hydrogen isotope compositions in clay minerals: a potential single-mineral geothermometer. Geochim. Cosmochim. Acta 60, 4285–4289.

Dill, H.G., Bosse, R., Henning, K.H., Fricke, A., Ahrendt, H., 1997. Mineralogical and chemical variations in hypogene and supergene kaolin deposits in a mobile fold belt the Central Andes of northwestern Peru. Miner. Deposita 32, 149–163.

Donnelly, T., Waldron, S., Tait, A., Dougans, J., Bearshop, S., 2001. Hydrogen isotope analysis of natural abundance and deuterium-enriched waters by reduction over chromium on-line to a dynamic dual inlet isotope-ratio mass spectrometer. Rapid Communication, Mass Spectrometry 15, 1297-1303.

Duzgoren-Aydin, N.S., Aydin, A., Malpas, J., 2002. Distribution of clay minerals along a weathered pyroclastic profile, Hong Kong. Catena 50, 17-41.

Fernández-Caliani, J.C., Galán, E., Aparicio, P., Miras, A., Márquez M.G., 2010. Origin and geochemical evolution of the Nuevo Montecastelo kaolin deposit (Galicia, NW Spain). Appl. Clay Sci. 49, 91-97.

Galán, E., Aparicio, P., Fernández-Caliani, J.C., Miras, A., Clauer, N., Fallick, A.E., 2013. Burela kaolin deposit (NW Spain). New insights on mineralogy and genesis. XV International Clay Conference, Rio de Janeiro.

Galán, E., Fernández-Caliani, J.C., Aparicio, P., Miras, A., Márquez, M.G., 2010 Mineralogical and geochemical constraints on the origin of the residual kaolin deposits derived from Variscan granitoids of Galicia (Spain).

SME Annual Meeting and Exhibit 2010, pp. 180-186.

Galán, E., Fernández-Caliani, J.C., Miras, A., Aparicio, P., Márquez, M.G., 2007. Residence and fractionation of rare-earth elements during kaolinization of alkaline peraluminous granites in NW Spain. Clay Miner. 42,341-353.

Galán, E., Ferrell, R.E., 2013. Genesis of Clays. In: Bergaya F., Lagaly G. (Eds.) Handbook of Clays Science. Developments in Clay Science vol. 5, Chapter 3, pp. 83-126.

Galán, E., Martín Vivaldi, J.L., 1972. Genetic classification of the Spanish kaolin deposits and their typology". In: Serratosa J.M. (Ed.) Proceedings of the 1972 International Clay Conference, Madrid, CSIC, Madrid, pp. 737-748.

Galán, E., Martín Vivaldi, J.L., 1973. Caolines españoles. Geología, mineralogía y génesis. Parte I. Bol. Soc. Esp. Ceram. Vidr. 12, 79-89.

~~Galán, E., Martín-Vivaldi, J.L., 1975. Caolines españoles. Geología, mineralogía y génesis. Parte VIII. Depósitos residuales y volcánicos. Bol. Soc. Esp. Ceram. Vidr. 14, 351-370.~~

Gilg, H.A., Hülmeyer, S., Miller, H., Sheppard, S.M.F., 1999. Supergene origin of the Lastarria kaolin deposit, south-central Chile, and paleoclimatic implications. Clays Clay Min. 47, 201–211.

Gilg, H.A., Sheppard, S.M.F., 1996. Hydrogen isotope fractionation between kaolinite and water revisited. Geochim. Cosmochim. Acta 60, 529–533.

Gouveia, M.A., Prudencio, M.I., Figueiredo, M.O., Pereira, L.C.J., Waerenborgh, J.C., Morgado, I. Pena, T., Lopes, A., 1993. Behaviour of REE and other trace and major elements during weathering of granitic rocks, Evora, Portugal. Chem. Geol. 107, 293-296.

Johnsson, M.J. 1993. The system controlling the composition of clastic sediments. In: Johnsson, M.J. & Basu, A. (eds) Processes controlling the composition of clastic sediments. Geological Society of America Special Paper 285, 1-19.

Julivert, M., Fontboté, J.M., Ribeiro, A., Conde, L.E., 1972. Mapa Tectónico de la Península Ibérica y Baleares a escala 1:1.000.000. Instituto Geológico y Minero de España, Madrid.

Laveuf, C., Cornu,S., 2009. A review on the potentiality of Rare Earth Elements to trace pedogenetic processes. Geoderma 154, 1-12.

Le Bas, M.J., Le Maitre, R.W., Streckeisen, A., Zanettin, B.,1986. A Chemical Classification of Volcanic Rocks Based on the Total Alkali-Silica Diagram. J. Petrology 27, 745-750.

Macaulay, C.I., Fallick, A.E., Haszeldine, R.S., Graham, C.M., 2000. Methods of laser-based stable isotope measurement applied to diagenetic cements and hydrocarbon reservoir quality. Clay Miner. 35, 317–326.

Márquez, M.G., Aparicio, P., Saverio, S., Galán, E., 2009. Determination of the kaolinite/halloysite ratio in kaolins using XRD and Dta/Tg.. XIV Internacional Clay Conference. Castellaneta Marina, Italia. 2009. Micro Et Nano: Sciantiae Mare Magnum, Vol I. 346. 346

Martínez-Catalán, J.R., Arenas, R., Díaz-García, F., Abati, J., 1997, Variscan accretionary complex of northwest Iberia: Terrane correlation and succession of tectonothermal events. Geology 25, 1103-1106.

Martín-Pozas, J.M., Galán, E., Martín-Vivaldi, J.L. 1971. Il giacimento di caolino di Jove,Lugo, Spagna. I Congresso Nazionale, AIPEA Italia. pp. 89–109.

Middelburg, J.J., Van der Weijden, C.H., Woittiez, J.R.W., 1988. Chemical processes affecting the mobility of major, minor and trace elements during weathering of granitic rocks. Chem. Geol. 68, 253–273.

Murray, H.H. 1988. Kaolin minerals: Their genesis and occurrences. In: Bailey S.W. (Ed.) Hydrous Phyllosilicates (Reviews in Mineralogy, 19), Mineralogical Society of America, Washington, DC, 67-89.

Nesbitt, H.W., 1979. Mobility and fractionation of rare earth elements during weathering of a granodiorite. Nature 279, 206- 210.

Panahi, A., Young, G.M., Rainbird, R.H., 2000. Behaviour of major and trace elements (including REE) during Paleoproterozoic pedogenesis and diagenetic alteration of an Archean granite near Ville Marie, Quebec, Canada. Geochim. Cosmochim. Acta 64, 2199–2220.

Papoulis, D., Tsolis-Katagas, P., Katagas C., 2004. Monazite alteration mechanisms and depletion measurements in kaolins. App. Clay Sci. 24, 271-285.

Pérez-Estaún, A., Bea, F. (Eds.), 2004. Macizo Ibérico. In: Geología de España (J.A. Vera, Ed.) SGE-IGME, Madrid, 19-230.

~~Pérez-Estaún, A., Martínez-Catalán, J.R., Bastida, F., 1991. Crustal thickening and deformation sequence in the football to the suture of the Variscan belt of Northwest Spain. Tectonophysics 191, 243-253.~~

~~Psyrillos, A., Burley, S.D., Manning, D.A.C., Fallick, A.E., 2003. Coupled mineral-fluid~~

~~evolution of a basin and high: kaolinitization in the SW England granites in relation to the development of the Plymouth Basin. In: Petford N. and McCaffrey K.J.W. (Eds.), Hydrocarbons in Crystalline Rocks. The Geological Society of London, Special Publications, 214, 175-195.~~

Putter, T.D., André, L., Bernard, A., Dupuis Ch, Jedwab, J., Nicaise, D., Perruchot, A., 2002. Trace element (Th, U, Pb, REE) 19ehavior in a cryptokarstic halloysite and kaolinite deposit from Southern Belgium: importance of “accessory” mineral formation for radioactive pollutant trapping. App. Geochem. 17, 1313–1328

~~Scheepers, R., Rozendaal A., 1993. Redistribution and fractionation of U, Th and rare-earth elements during weathering of subalkaline granites in SW Cape Province, South Africa. J. African Earth Sci 17, 41-50.~~

Schultz, L.G. 1964. Quantitative interpretation of mineralogical composition from X-ray and chemical data for the Pierre shale. U.S. Geological Survey Professional Paper, p. 391C.

Sheppard, S.M.F., Gilg, H.A., 1996. Stable isotope geochemistry of clay minerals. Chem. Geol. 31, 1–24.

Sheppard, S.M.F., Nielsen, R.L., Taylor Jr., H.P., 1969. Hydrogen and oxygen isotope ratios of clay minerals from porphyry copper deposits. Econ. Geol. 66, 515–542.

~~Wilson, I.R., 1998. Kaolin deposits of Western Iberia. Geoscience in South-West England, 9, 214-217.~~

CAPTIONS OF TABLES AND FIGURES

TABLES

Table 1.- Mineralogical and chemical analysis (major elements in %wt) for the representative rocks of the deposit.

Table 2.- Chemical analysis (trace elements in mg/kg) for the representative rocks of the deposit.

Table 3.- Mineralogical and chemical composition (%wt) for the bulk kaolins.

Table 4.- Mineralogical composition (%wt) of the finer fractions.

Table 5. Chemical composition (major elements in wt%) of the finer fractions.

Table 6. Chemical composition (trace elements in mg/kg) of the bulk samples.

Table 7. Chemical composition (trace elements in mg/kg) of the finer fractions.

Table 8.- H_2O yields, $\delta^{18}O$ and δ D values of the analyzed <1μm size fractions, and $\delta^{18}O$ and δ D average values of the separates with the same sizes.

FIGURES

Figure 1.- Regional geological map of Galicia (NW Spain) after Martinez-Catalán et al. (1997) showing the location of the studied kaolin deposit.

Figure 2.- Panoramic view of the kaolin quarries at Ramón-Fazouro and sketch of the sample location in the studied outcrops.

Figure 3. a) Micro-photographs of felsite (RF-8) showing feldspars crystals in a microcrystalline matrix composed of plagioclase, quartz, muscovite and biotite; b) micaschist (RF-2) showing oriented micaceous minerals bands alternating with quartz plus feldspars bands; c) quartzite (RF-3) (polygonal quartz grains). PXA, 4x.

Figure 4.- a) Halloysite joined to book-like kaolinite aggregate; (b and e)Kaolinite crystals oriented face to face; (c) halloysite crystals in clusters; (d) Halloysite in tubular shape with kaolinite crystals oriented face to face; (f) tubular halloysite crystals and spherical particles which could be allophane.

Figure 5.- a) Major chemical composition normalized to felsite; b) normalized to metapelite.

Figure 6.- a) Trace elements composition normalized to felsite; b) normalized to metapelite.

Figure 7.- a) Felsite normalized REE distribution pattern of the kaolin samples; b) felsite-normalized REE distribution patterns of different grain-size fractions of the same sample.

Figure 8. Cluster analysis.

Figure 9. $\delta^{18}O$ versus δD diagram for the <1 μm fraction of the kaolin. The meteoric water, supergene/hypogene and kaolinite weathering lines (KWL) are given for reference. The dashed line indicates the oxygen and deuterium isotopic composition of water in equilibrium with a kaolinite with the mean isotope ratios ($\delta^{18}O$= 20.4‰ and δD= -74‰). Abundances are expressed as parts per thousand relative to Vienna Standard Mean Ocean Water (V-SMOW).

Figure 10.- Some pictures realized during the visit of Prof. Haydn Murray to Burela kaolin deposit and Sargadelos Ceramic factory (2005) with some of the authors of this paper.

NEW INSIGHTS ON MINERALOGY AND GENESIS OF KAOLIN DEPOSITS: THE BURELA KAOLIN DEPOSIT (NORTHWESTERN SPAIN)

Emilio Galan[1], Patricia Aparicio[1], Juan Carlos Fernández-Caliani[2], Adolfo Miras[1], Marcial G. Márquez[1], Anthony E. Fallick[3], Norbert Clauer[4].

[1] Departamento Cristalografía, Mineralogía, y Química Agrícola, Facultad de Quimica, University of Sevilla, Spain

[2] Departamento de Geologia, Facultad de Ciencias Experimentales, University of Huelva, Spain[3] Scottish Universities Environmental Research Centre, East Kilbride, Glasgow G75 0QF, UK

[4] Laboratoire d'Hydrologie et de Géochimie de Strasbourg (CNRS-UdS), University of Strasbourg, France

CORRESPONDING AUTHOR: Patricia Aparicio **paparicio@us.es**

NEW INSIGHTS ON MINERALOGY AND GENESIS OF KAOLIN DEPOSITS: THE BURELA KAOLIN DEPOSIT (NORTHWESTERN SPAIN)

E. Galan[1], P. Aparicio[1], J.C. Fernández-Caliani[2], A. Miras[1], M.G. Márquez[1], A.E. Fallick[3], N. Clauer[4].

[1] Departamento Cristalografía, Mineralogía, y Química Agrícola, Facultad de Quimica, University of Sevilla, Spain

[2] Departamento de Geologia, Facultad de Ciencias Experimentales, University of Huelva, Spain[3] Scottish Universities Environmental Research Centre, East Kilbride, Glasgow G75 0QF, UK

[4] Laboratoire d'Hydrologie et de Géochimie de Strasbourg (CNRS-UdS), University of Strasbourg, France

ABSTRACT

The Burela deposit is the largest kaolin deposit in Spain, mined for more than 50 years, the product being mainly used for porcelain. Kaolin is dominantly associated with Lower Cambrian felsites, interbedded with quartzites, micaschists and metapelites (Cándana Series), and was strongly folded during the Hercycian orogeny. Kaolin layers were ductile and incompetent materials among more competent ones, producing many slides with a diastrophic appearance. Consequently, kaolin outcrops are morphologically very variable, -i.e. pockets -, and interlayered between metapelites and/or quartzites, resulting in complication for prospection and mining.

The kaolin consists mainly of kaolinite, tubular halloysite, and spherical allophane along with quartz and minor illite. The content of kaolin minerals reaches up to 90% in the finer fraction (<2μm and <1μm).

Geochemical analyses of trace and REE show a close relationship between kaolin and associated rocks. Two kaolin types can be differentiated: (i) massive, associated to felsite; and (ii) related to metapelite. A temperature range from 20 to 35°C, with an average of approximately 28ºC was calculated on the basis of the isotopic signatures ($\delta^{18}O$, δ D) for the kaolin materials. This scatter suggests that if continental weathering was involved in the kaolin formation on the lower side of the temperatures, it was not the only process, especially for kaolin associate with felsites and metapelites. The higher temperatures are indicative of a hydrothermal auto-metamorphic alteration, followed by a folding of the series that induced an apparently chaotic kaolin distribution with a combined continental weathering superimposed on the previous low-temperature hydrothermal felsite transformation.

Key words: kaolin genesis, trace elements, isotopes, halloysite, Galicia, Spain

INTRODUCTION

The origin of primary kaolin deposits is usually a matter of controversy because kaolinite can be formed *in situ* by weathering reactions (supergene kaolins), hydrothermal alteration during the late stages of magma cooling (hydrothermal kaolins), or by a combination of both processes (Murray, 1988). Kaolinite can be formed also within sedimentary continental basins by diagenetic processes (Galán and Ferrell, 2013). Various criteria and indicators have been proposed to distinguish supergene from hypogene kaolins (e.g. Dill et al., 1997, Gilg et al., 1999), although some of them are considered as ambiguous. Unravelling the genesis of kaolinite in deeply weathered magmatic rocks is one of the most important challenges faced by clay geologists.

In the Variscan belt of Galicia (NW Spain) kaolinization of crystalline rocks is widespread. Large high-grade deposits of kaolin (e.g. Vimianzo, Nuevo Montecastelo) and other minor occurrences are found in association with weathered granites. The combined oxygen and hydrogen isotope composition of kaolinite from such deposits is consistent with data of supergene kaolin formation (Clauer et al., 2010, 2015; Fernández-Caliani et al., 2010). However, some deposits associated with felsite dykes or sills and quartz vein networks could have

been formed *in situ* by complex fluid/rock hydrothermal and supergene interactions.

The Burela kaolin deposit (Northern Galicia) is a volcanic-hosted deposit, which is of particular interest in addressing the origin and timing of kaolinization. Volcanic-hosted kaolin occurrences of no current economic interest are also found in other areas of Spain, such as the Canary Islands and within the volcano-sedimentary complex of the Iberian Pyrite Belt. However it is in the Burela area where kaolinization is best represented. The deposit is geologically located (Fig. 1) in the West Asturian-Leonese Zone (WALZ), one of the major tectono-stratigraphic terranes into which the Iberian Massif is classically subdivided (Julivert et al., 1972). The WALZ exposes Precambrian to Devonian metasediments that experienced the effects of the Variscan orogeny between Late Devonian and Late Carboniferous times (Martínez-Catalán et al., 1997; Pérez-Estaún and Bea, 2004).

The main Burela quarries are San Andrés and Ramón Fazouro that are located near the western edge of Fazouro village (Fig. 1). The kaolin is spatially and genetically related to felsites and a swarm of quartz-porphyry dykes that intruded Lower Cambrian metasediments. Kaolin is dominantly associated with Lower Cambrian felsites, interbedded with quartzites and sandstones, and metapelites (Cándana Series), and which were strongly folded during the Hercynian orogeny. Kaolin-rich layers became a ductile and incompetent materials interleaved among the more competent ones, producing many slides with a diastrophic appearance. Consequently, the kaolin outcrops are morphologically very variable (i.e. pockets) interlayered between other rocks, resulting in difficult prospection and mining.

This world-class kaolin deposit has been mined by ECESA for more than half a century (1957-2014), with the kaolin being mainly used as raw material in the manufacture of high quality ceramics, especially porcelain-ware. The kaolin material consists of a mixture of kaolinite and halloysite with minor allophane (Galán et al., 2013). The origin of this important economic deposit is still an ongoing matter of debate. It is unclear if extensive kaolinization resulted from hydrothermal (by meteoric fluids) alteration of felsitic rocks, or if weathering affected material that was already subjected to a first stage of low grade metamorphism, or a combination of the two processes induced the deposit

(Galán and Martín Vivaldi, 1972). The aim of this paper is to revisit the arguments first presented, (i.e. hydrothermal alteration by meteoric fluids), on the basis of new insights from mineralogy, trace-element geochemistry and stable isotope data. Such understanding will be helpful for future exploration for new deposits in the region and to the rationalization of mining operations.

SAMPLING AND ANALYTICAL METHODS

A representative sampling of the Burela kaolin deposit was undertaken in the Ramón Fazouro quarry (Fig. 2). A total of forteen samples of different kaolin occurrences and their associated rocks were sampled. Three size fractions (<45, <2 and <1 μm) were extracted from each whole rock by wet sieving, sedimentation in distilled water and centrifugation. The size fractions were mineralogically analysed by X-ray diffraction (XRD) on a Bruker D8 Advance instrument with a scanning speed of 0.5º(2θ)/min, 0.15 step/size, and Cu-kα radiation (40 kV, 30 mA). The quantitative composition was carried out following the procedures of Schultz (1964), Martín-Pozas et al. (1971) and Galán and Martín Vivaldi (1973) for the whole kaolin and the <45 and <2μm fractions. In order to resolve the unequivocal identification of kaolinite and halloysite from the XRD patterns, and to provide a method of quantification in these types of samples, a fitting process was applied to the 002 XRD reflections (~3.5 Å), using a pseudovoight function for minimising the effect of the Lorentz-Polarization factor, since this signal appears at relatively high angles (24-26º) (Márquez et al, 2009).

The Rietveld method was used with the TOPAS program to evaluate the mineralogical composition of the <1μm separates, to obtain a very precise mineralogical composition for this size fraction, potentially the least modified by contaminant minerals, and to quantify the proportions of the different kaolin minerals (e.g. kaolinite vs. halloysite). This procedure was applied to the <1μm fraction to relate the isotopic with the mineralogical data.

A few samples (5) were selected for high-resolution observation by a scanning electron (HRSEM) HITACHI S5200 instrument, fitted with an EDS detector. The particle morphology was also studied by atomic force microscopy with a Pico Plus

instrument. In addition the country rocks were optically examined under polarizing photomicroscope. X-ray analyses and microscopy observations were performed at the CITIUS (Research Facilities Centre at the University of Seville, Spain).

For the bulk sample and <45 and <2 μm fractions, chemical analyses were carried out at the Activation Laboratories Ltd. (Ontario, Canada) following a lithium metaborate/tetraborate fusion technique that ensures dissolution of the entire sample. Major-element concentrations were determined by inductively coupled plasma-optical emission spectrometry (ICP-OES) on a Thermo Jarrell Ash ENVIRO II, and trace elements were analyzed by inductively coupled plasma-mass spectrometry (ICP-MS) on a Perkin Elmer Optima 3000. Quality control included the use of several certified reference materials, duplicates and blanks by the laboratory to check accuracy and precision. The chemical results were statistically treated in order to realize cluster analysis.

The mineralogical maturity of weathering was estimated using the mineralogical index alteration (MIA; Johnsson, 1993; Nesbitt et al., 1996), which is a dimensionless number between 0 and 100, calculated from mineral weight percentages derived from XRD analysis as follows:

$$MIA = [quartz / (quartz + K\text{-feldspar} + plagioclase)] \times 100$$

The chemical index of alteration (CIA, Nesbitt and Young, 1982) was calculated to evaluate the degree of chemical weathering. CIA is also a dimensionless number between 0 and 100, and shows the weathering of feldspar minerals. It is calculated using molecular proportions as follows:

$$CIA = [Al_2O_3/(Al_2O_3+CaO^*+Na_2O+K_2O)] \times 100$$

where CaO* presents the amount of CaO combined in the silicate fraction of the rock.

The stable isotope data were obtained in two different laboratories. In both places, samples were vacuum-degassed at 200ºC overnight to remove the interlayer and absorbed surface water prior to hydrogen isotope analysis. Then, they were transferred to an out-gassed Pt crucible and the water released by heating was reacted with hot metal, producing H_2 for determination of δD. For the samples analysed at the Activation Laboratories (Canada), uranium at 900°C was

used for D/H; for $\delta^{18}O$ analysis, BrF_5 at 650°C was reacted with the kaolin in a Ni chamber (Clayton and Mayeda, 1963) to generate O_2 that was reduced to CO_2 with graphite using Pt as catalyst at 550-600ºC. The precision at 1σ was ± 2‰ and 0.3‰ respectively for δD and δ18O. For those results obtained at East Kilbride (UK), dehydroxylation was achieved by heating the Pt crucible at 1200ºC by radiofrequency induction. The water released was converted to H_2 by reacting with Cr at 800ºC (Bigeleisen et al., 1952; Donnelly et al., 2001) in a multiple-pass system. The H_2 yield was measured manometrically and the δD determined on a gas-source mass spectrometer calibrated via water and mineral standards. Using these techniques, the NBS30 biotite standard gave a δD of -65‰ (V-SMOW) with an analytical reproducibility of ± 2‰ (1σ), ± 3‰ (1σ) being more appropriate for clay material. The oxygen isotope composition was determined by laser fluorination (Macaulay et al., 2000) using the Borthwick and Harmon (1982) ClF_3 modification of Clayton and Mayeda (1963). The precision for the clay material is ± 0.3‰ (1σ), the NBS28 quartz standard giving a $\delta^{18}O$ of 9.6‰ (V-SMOW). All clay isotope data are reported in parts per mil (‰) relative to the V-SMOW standard. No significant systematic isotope ratio difference between the two laboratories was observed. Stable isotopes were determined for four samples <45 μm fraction and eight samples <2 and <1μm fractions.

RESULTS AND DISCUSSION

Precursor host rocks

The Burela kaolin deposit is hosted in felsic porphyritic volcanic rocks interbedded with metasedimentary rocks, notably Lower Cambrian metapelites and quartzites (Cándana Quartzite). Representative mineralogical and chemical analyses of the precursor rocks of the kaolin deposit are given in Tables 1 and 2.

In thin section the felsic volcanic rocks display a holocrystalline, porphyritic texture (Fig. 3a), with phenocrysts of feldspar and patially reabsorbed quartz and set in a groundmass composed of fine-grained plagioclase, muscovite, and biotite

(often altered to chlorite and associated to iron oxides). Quantitative XRD mineralogical determination showed that quartz accounts for 24-33% of the bulk sample, the feldspars range from 60 to 67%, with mica contents up to 30%. In partially altered samples, the amount of feldspars decreases by up to 35% yielding MIA values of 46. According to the TAS binary diagram (total silica **vs** alkali content) of Le Bas et al. (1986), the felsic rocks can be classified as lavas of rhyolite-to-trachydacite composition.

The pelitic schists have a lepidoblastic texture and exhibit a strong penetrative foliation defined by preferred orientation of muscovite laths and quartz ribbons (Fig. 3b). Chlorite and relict detrital grains of tourmaline, rutile and zircon are present as accessory phases. Intensely altered metapelitic rocks (MIA value as high as 87) are characterized by high content of clay minerals, notably kaolinite, which can account for up to 38% (Table 1).

The Cándana quartzite shows a medium-grained granoblastic texture, in which quartz exhibiting undulate extinction typically forms a mosaic of polygonal crystals (Fig. 3c), with muscovite, tourmaline, zircon and rutile as subordinate minerals].

Mineralogical characteristics of kaolin.

The mineralogy of the bulk samples is dominated by highly variable contents of kaolin minerals (17-74%) and quartz (16-69%), accompanied by mica (up to 33%) (Table 3). Other phases that may be present, usually in subordinate or trace amounts, are feldspars and smectites. Additionally, SEM-BSE observations in combination with EDS microanalysis revealed a distinctive suite of heavy minerals including zircon, monazite, rutile, ilmenite and iron oxides.

Within the <45μm fraction, the amounts of kaolin minerals is variable with a wide concentration range (62-90%), with kaolinite being dominant over halloysite. The contents of quartz and illite were lower than 24% in all the samples, whereas feldspars, smectites and allophane were found as accessory phases. In the fine fractions, the amount of kaolin minerals reached up to 92 % (Table 4). Traces of allophone and chlorite were detected in some samples and fractions. The

fractions <2μm and <1μm contains mostly kaolinite and halloysite, with minor illite and quartz (Table 4).

Tubular halloysite accounts for 11 to 60% of the kaolin, while kaolinite content varies between 23 and 60%, with kaolinite/halloysite ratios ranging from 6 to 0.5. These results substantially agree with the microscopic observations (Figure 4). Tubular crystals of halloysite (0.5-8μm of length) appear to be joined to book-like kaolinite aggregates (Figure 4a, 4e and 4f) and kaolinite crystals are oriented face to face (Fig 4 b and 4d). Halloysite crystals appear also in the form of clusters (Fig 4c). Spherical shaped particles (0.5μm in diameter) were also detected by AFM, which correspond to allophane: it is not common to find at the same time tubular and spherical halloysite (Fig 4f). Tubular halloysite mostly corresponds to a weathering phase while spherical halloysite is instead formed by direct precipitation (neoformation) and it is usually considered as a precursor of tubular halloysite (Duzgoren-Aydin et al. 2002).

Major and trace element geochemistry

Chemical analyses of the whole rock samples shows that the geochemistry of major elements (Table 3) is largely dominated by Si and Al, reflecting the high content of kaolin minerals in the altered rocks. Silica displays a broad range of concentrations (58.2-76.3 wt % SiO_2), except for the altered quartzite (RF-12), which is also strongly and negatively correlated with both the alumina content (r= -0.99) and the weight loss on ignition (LOI; r= -0.88). The highest abundances of alumina (23-27 wt % Al_2O_3) and LOI (8-12 wt %) were found in samples from the upper part of the studied section.

The remaining major elements, except potassium, are all present at concentrations less than 1wt%. The K_2O content varies from 4.8wt% to 0.8wt%, with a mean value of 2.3wt%. The variations are closely related to the presence of orthoclase and muscovite in the samples. The low content of calcium and sodium oxides is considered due to weathering of the plagioclases. The CIA varies from about 65 in the fresh felsitic rocks to around 96 in the most weathered felsite, suggesting a significant removal of labile basic cations (mainly K, Na, and

Mg) relative to stable residual elements (Si, Al, Fe). The loss of alkaline and alkaline-earth elements can be attributed to the alteration (kaolinization) of alkali feldspar and mica, which are the minerals in the felsitic rocks most prone to weathering. In addition, the CIA of the metapelite is 84%, which indicates that this rock is highly altered, as confirmed by the high kaolin minerals content (31wt%).

The fine-grained kaolin rich samples (the <45 and <2μm fractions) contain a higher proportion of alumina (up to 37 wt % Al_2O_3) and concomitantly less silica (44-59 wt %) (Table 5). An enrichment in titanium oxide is detected in metapelite (RF-2) and in the samples RF3-05, RF-12 and RF-14, when the major elements composition is normalized to felsite (RF-8) (Figure 5a). As was noted above, the metapelite presents abundant rutile. The other kaolin samples do not contains any significant anomaly in comparison with the felsite host rock.

When the major element compositions of samples RF3-05, RF-12 and RF-14 are normalized to the metapelite reference (Figure 5b), no striking anomaly is visible and the signatures of the samples are very similar to metapelite. The unexpectedly high anomaly is of 2.5 in the case of iron oxide for <45μm fraction of sample RF-14.

An enrichment in the high field strength elements (HFSE) Sc, Zr, Hf and Th has been detected in kaolin when the data are normalized to felsite (RF-8) (Figure 6a), probably due to their resistance to weathering (e.g. Middelburg et al., 1988; Panahi et al., 2000). Thus the HFSE remained relatively immobile, linked to resistant heavy minerals (zircon, monazite and titanium oxides) that tend to be residually concentrated in the finer fractions of the kaolin. A very high statistical correlation (r= 0.97) was obtained between Zr and Hf, so that both elements mostly reside in the crystal structure of zircon. Elevated correlation coefficients were also observed between Nb and Ta (r= 0.88) because of the close geochemical affinity of such elements. Thorium shows a positive correlation (r= 0.65) with the light rare earth elements (LREE) consistently indicating that it is hosted by monazite, which is the only LREE-rich accessory phase occurring in the kaolin.

High enrichments for large ion lithophile elements (LILE), such as Rb, Sr and Cs, are found in relation to metapelite for the samples RF-12 and RF-14, especially

in the <45μm fraction (Figure 6b). But, when the trace-element compositions of samples RF-3-05, RF-12 and RF-14 are normalized to the metapelite composition, no anomaly is apparent with the signature of these samples very similar to that of the metapelite. On the contrary, the major anomalies are for Cs, Tl, Pb, Rb, Sr and Ta of the felsite and the other kaolin samples. The LILE probably were preferentially removed from the felsite rock during kaolinization, as noted by the depletion of Rb, Sr, and particularly Ba, in the kaolin.

The kaolin is not especially enriched in trace elements, although the overall abundance varies with the grain-size distribution (Tables 6 and 7). The <45μm fraction of the kaolin tends to have greater concentrations (ΣREE= 237-440 ppm) than the whole sample (ΣREE= 65-209 ppm), indicating a relative accumulation of REE-carrying minerals in the finer fractions. Seemingly, kaolinite could have played a role in scavenging REE, as reported in some weathering systems (Putter et al., 2002; Papoulis et al., 2004). Exceptionally, the sample RF-17 is markedly depleted in total REE (whole sample: 29 ppm; <45μm fraction: 37 ppm; <2μm fraction: 85 ppm) relative to the felsite rock, although the REE concentration level also exhibits the same dependence on the particle size of the kaolin.

Similar overall enrichments in REE have been documented in weathering profiles developed on granitoids elsewhere in the Galician region (Galán et al., 2007, Fernández-Caliani et al., 2010). However, at the Burela deposit the total REE content shows no significant correlation with the intensity of the chemical alteration (as shown by the CIA values), suggesting that other processes of remobilization and redistribution of REE occurred in this deposit. In addition, all the samples yield a similar pattern of the REE composition: in fact the shape of the REE patterns is identical for all grain-size fractions, characterized by a slight LREE enrichment (La_n/Sm_n=3.50-13.56) and a HREE depletion (Gd_n/Yb_n= 1.70-5.24). The positive Ce anomaly is due to the residual character of this element, which undergoes only partial oxidation (Gouveia et al., 1993).

The REE diagrams of the kaolin whole samples normalized against the fresh felsite (Fig. 7a) exhibit a nearly flat pattern with a slight enrichment in heavy REE (HREE), which is more prominent in the fine-grained samples (Fig. 7b). The HREE distribution seems to be controlled, therefore, by HREE-enriched phases

like zircon, ilmenite, and rutile (Laveuf and Cornu, 2009). These resistant minerals are not expected to be highly mobilized during alteration, and therefore they tend to be residually accumulated in the kaolin deposit, thus increasing the HREE budget. A cluster analysis identifies two types of geochemical signature (trace elements and REE) and the massive kaolin samples can be grouped into two main groups: associated to felsite and associated to metapelite (Figure 8).

In summary, the geochemical study of trace elements and REE showed a close relationship between kaolin and associated rocks, and from the geochemical point of view two kaolin types can be differentiated: massive kaolin associated to felsite and massive kaolin associated to metapelite, as above it has been largely discussed.

Stable isotope geochemistry

Combined stable oxygen and hydrogen (deuterium) isotope studies are commonly used to help discriminate between supergene and hypogene kaolins, and are considered to be the most powerful method to constrain temperatures of kaolinization (Gilg, et al. 1999).

The isotopic composition of nearly pure kaolin samples (<1μm fraction) from Burela deposit showed a narrow range of $\delta^{18}O$ values (19.8-21.0‰) and δD ratios ranging from -85 to -63‰, with the mean $\delta^{18}O$ and δD values being 20.4±0.4‰ and -74±3‰, respectively (Table 8). The scatter is close to the analytical error, indicating little geological variation. There is no statistically significant correlation between the two isotope ratios (r = -0.39, less than 80% significant for n=7). The mean water content of 7.4±0.4wt.% corresponds to 13.3±0.7 μmoles mg^{-1} of water, compared to the theoretical value of 14 for stoichiometric kaolin.

When plotted on a $\delta^{18}O$- δD diagram (Fig.9), all the points plot in the supergene field, *i.e.* on the right of the supergene-hypogene line of Sheppard et al. (1969), and very close to the kaolinite weathering line (KWL), which represents the isotopic compositions of kaolinites in equilibrium with meteoric waters at 20 °C. Similar values are given in the literature for residual kaolin deposits derived from

Variscan granites (Bobos and Gomes, 1998; Boulvais et al., 2000; Clauer et al., 2010, 2015; Fernández-Caliani et al., 2010; Galán et al., 2010). Here, the overall range of the calculated temperatures from studied kaolin separates ranges from 20 to 35 °C. These temperatures are compatible with a low-temperature hydrothermal activity, i.e.: a hydrothermal auto-metamorphic alteration that could occur on the felsite during submarine volcanic activity.

On the basis of a variety of assumptions involving plausible formation in an open system with high water–rock ratio and near-surface temperatures, a comparison with Delgado and Reyes (1996) modelling appears appropriate at this point, remembering that these authors assume an interaction with meteoric waters. Thus, the temperature and isotopic composition of the water from which kaolinite formed in equilibrium can be determined from the following equations:

[1] The meteoric-water equation: $\delta D = 8\delta^{18}O + 10$ (Craig, 1961)

[2] The equilibrium hydrogen isotope fractionation factor (α^{H}) between kaolinite and water (Gilg and Sheppard, 1996): $1000 \ln \alpha^{H}_{\text{kaol-water}} = -2.2 \times 10^{6}\, T^{-2} - 7.7$

[3] The equilibrium oxygen isotope fractionation factor (α^{18}) between kaolinite and water (Sheppard and Gilg, 1996): $1000 \ln \alpha^{18}_{\text{kaol-water}} = 2.76 \times 106\, T^{-2} - 6.75$.

In combining the equations of Sheppard and Gilg (1996) for kaolinite, $\delta^{18}O_w$, δD_w can be eliminated by using the meteoric water line equation, giving:

$$3.04\ 10^{6}\ T^{-2} = \delta^{18}O_k - 0.125\ \delta D_k + 7.04$$

The crystallization temperature of kaolinite obtained by applying this equation to the average of the measured <1 μm kaolin separates at 14.7 ºC is compatible with the supergene environment. This value is slightly higher than the current annual mean temperature of the Galician region (12 °C), but is a reasonable surface temperature expected during the Pliocene (Boulvais et al., 2000), with an accuracy of the equations representing the temperature dependence of the stable isotope fractionation equations (in (2) and (3) above) not at all well quantified.

The possible mean isotopic composition of the meteoric water with which kaolinite crystallized at isotopic equilibrium has been calculated at $\delta^{18}O$ = -6‰ and δD = -40‰ (Fig. 9; mean values for the minerals taken from Table 8), using the above average temperature and the isotope fractionation factors of Sheppard and Gilg (1996) and Gilg and Sheppard (1996), respectively.

CONCLUSIONS

The Burela deposit is characterized by a high concentration of kaolin minerals (kaolinite and halloysite). In the coarse fraction the most abundant kaolin mineral is kaolinite of perfect pseudo-hexagonal morphology. Tubular halloysite is concentrated in the finer fractions.

The geochemical study of the trace elements and REE showed a close relationship between kaolin and associated rocks, and from the geochemical point of view two kaolin types can be differentiated: associated to felsite and associated to metapelite.

A felsite hydrothermal auto-metamorphic alteration is suggested for the origin of the kaolin, as an initial kaolinization step. Later a folding of the series led to an apparently chaotic kaolin distribution and a weathering action on the felsite completed the kaolin formation, superimposed on a low-temperature hydrothermal felsite transformation. On the contrary, the occurrence of allophone in some samples point toward a supergene origin of the kaolin. On the other hand, micaschists were also kaolinized by weathering. The kaolin was a plastic incompetent material during the folding, which accumulated in the weaker zones, and was a detachment level for the more competent materials (mainly quartzite and sandstone).

The isotopic composition of the nearly pure kaolin is consistent with a supergene origin. The mean $\delta^{18}O$ and δD values of the <1 μm fraction indicate that the most likely scenario is formation in equilibrium with meteoric waters at near surface temperatures (between 20 and 36°C). The scenario of a continental weathering followed by a low-temperature hydrothermal episode is therefore plausible.

These new insights into the genesis of the Burela volcanic-hosted kaolin deposit may provide useful information to guide kaolin regional exploration.

ACKNOWLEDGEMENTS

This work has been partially supported by the Spanish Ministry of Education and Science (Project BET2001-2415) and the Government of Andalusia through the Research Group Applied Mineralogy (RNM135). Authors are indebted to Dr. Collin Harvey and an anonymous reviewer for constructive and improving comments. Authors are grateful to Haydn H. Murray for his advice and kind collaboration during the field research (Figure 10).

REFERENCES

Bigeleisen, J., Perlman, M.L., Prosser, H.C., 1952. Conversion of hydrogenic materials to hydrogen for isotopic analysis. Anal. Chem. 24, 356-1357.

Bobos, I., Gomes, C., 1998. Greisen and post-greisen alteration of the Sao Vicente de Pereira kaolinite deposit, Portugal. Can Mineral, 36, 1615-1624.

Borthwick, J., Harmon, R.S., 1982. A note regarding ClF_3 as an alternative to BrF_5 for oxygen isotope analysis. Geochim. Cosmochim. Acta 46, 1665-1668.

Boulvais, P., Vallet, J.M.,, Estéoule-Choux,J., Fourcade, S., Martineau, F., 2000. Origin of kaolinization in Brittany (NW France) with emphasis on deposits over granite: stable isotopes (O, H) constraints. Chem. Geol. 168, 211–223

Clauer, N., Fallick, A.E., Galán, E., Aparicio, P., Miras, A., Fernandez-Caliani J.C., Aubert A. 2015. Stable isotope constraints on the origin of kaolin deposits from Variscan granitoids of Galicia (NW Spain). Chem Geol., 417, 90-101.

Clauer, N., Galán, E., Fallick, A.E., Fernández Caliani, J.C., Aparicio, P., Márquez, M.G, Miras A. 2010. Stable isotope constraints on the origin of kaolin deposits from variscan granitoids and felsites, and from sedimentary basins of galicia (NW Spain).Pp 97-98 in M.C. Hermosin, R. Celis, F. Bruna and P. Aparicio (editors) 2010 SEA-CSSJ-CMS Trilateral Meeting Books of Abstract of General Meeting.

Clayton, R.N., Mayeda, T.K., 1963. The use of bromine pentafluoride in the extraction of oxygen in silicates for isotopic analysis. Geochim. Cosmochim. Acta 27, 43-52.

Craig, H., 1961. Isotopic variations in meteoric waters. Science 133, 1702–1703.

Delgado, A., Reyes, E., 1996. Oxygen and hydrogen isotope compositions in clay minerals: a potential single-mineral geothermometer. Geochim. Cosmochim. Acta 60, 4285–4289.

Dill, H.G., Bosse, R., Henning, K.H., Fricke, A., Ahrendt, H., 1997. Mineralogical and chemical variations in hypogene and supergene kaolin deposits in a mobile fold belt the Central Andes of northwestern Peru. Miner. Deposita 32, 149–163.

Donnelly, T., Waldron, S., Tait, A., Dougans, J., Bearshop, S., 2001. Hydrogen isotope analysis of natural abundance and deuterium-enriched waters by reduction over chromium on-line to a dynamic dual inlet isotope-ratio mass spectrometer. Rapid Communication, Mass Spectrometry 15, 1297-1303.

Duzgoren-Aydin, N.S., Aydin, A., Malpas, J., 2002. Distribution of clay minerals along a weathered pyroclastic profile, Hong Kong. Catena 50, 17-41.

Fernández-Caliani, J.C., Galán, E., Aparicio, P., Miras, A., Márquez M.G., 2010. Origin and geochemical evolution of the Nuevo Montecastelo kaolin deposit (Galicia, NW Spain). Appl. Clay Sci. 49, 91-97.

Galán, E., Aparicio, P., Fernández-Caliani, J.C., Miras, A., Clauer, N., Fallick, A.E., 2013. Burela kaolin deposit (NW Spain). New insights on mineralogy and genesis. XV International Clay Conference, Rio de Janeiro.

Galán, E., Fernández-Caliani, J.C., Aparicio, P., Miras, A., Márquez, M.G., 2010 Mineralogical and geochemical constraints on the origin of the residual kaolin deposits derived from Variscan granitoids of Galicia (Spain).

SME Annual Meeting and Exhibit 2010, pp. 180-186.

Galán, E., Fernández-Caliani, J.C., Miras, A., Aparicio, P., Márquez, M.G., 2007. Residence and fractionation of rare-earth elements during kaolinization of alkaline peraluminous granites in NW Spain. Clay Miner. 42,341-353.

Galán, E., Ferrell, R.E., 2013. Genesis of Clays. In: Bergaya F., Lagaly G. (Eds.) Handbook of Clays Science. Developments in Clay Science vol. 5, Chapter 3, pp. 83-126.

Galán, E., Martín Vivaldi, J.L., 1972. Genetic classification of the Spanish kaolin deposits and their typology". In: Serratosa J.M. (Ed.) Proceedings of the 1972 International Clay Conference, Madrid, CSIC, Madrid, pp. 737-748.

Galán, E., Martín Vivaldi, J.L., 1973. Caolines españoles. Geología, mineralogía y génesis. Parte I. Bol. Soc. Esp. Ceram. Vidr. 12, 79-89.

Gilg, H.A., Hülmeyer, S., Miller, H., Sheppard, S.M.F., 1999. Supergene origin of the Lastarria kaolin deposit, south-central Chile, and paleoclimatic implications. Clays Clay Min. 47, 201–211.

Gilg, H.A., Sheppard, S.M.F., 1996. Hydrogen isotope fractionation between kaolinite and water revisited. Geochim. Cosmochim. Acta 60, 529–533.

Gouveia, M.A., Prudencio, M.I., Figueiredo, M.O., Pereira, L.C.J., Waerenborgh, J.C., Morgado, I. Pena, T., Lopes, A., 1993. Behaviour of REE and other trace and major elements during weathering of granitic rocks, Evora, Portugal. Chem. Geol. 107, 293-296.

Johnsson, M.J. 1993. The system controlling the composition of clastic sediments. In: Johnsson, M.J. & Basu, A. (eds) Processes controlling the composition of clastic sediments. Geological Society of America Special Paper 285, 1-19.

Julivert, M., Fontboté, J.M., Ribeiro, A., Conde, L.E., 1972. Mapa Tectónico de la Península Ibérica y Baleares a escala 1:1.000.000. Instituto Geológico y Minero de España, Madrid.

Laveuf, C., Cornu,S., 2009. A review on the potentiality of Rare Earth Elements to trace pedogenetic processes. Geoderma 154, 1-12.

Le Bas, M.J., Le Maitre, R.W., Streckeisen, A., Zanettin, B.,1986. A Chemical Classification of Volcanic Rocks Based on the Total Alkali-Silica Diagram. J. Petrology 27, 745-750.

Macaulay, C.I., Fallick, A.E., Haszeldine, R.S., Graham, C.M., 2000. Methods of laser-based stable isotope measurement applied to diagenetic cements and hydrocarbon reservoir quality. Clay Miner. 35, 317–326.

Márquez, M.G., Aparicio, P., Saverio, S., Galán, E., 2009. Determination of the kaolinite/halloysite ratio in kaolins using XRD and Dta/Tg.. XIV Internacional Clay Conference. Castellaneta Marina, Italia. 2009. Micro Et Nano: Sciantiae Mare Magnum, Vol I. 346. 346

Martínez-Catalán, J.R., Arenas, R., Díaz-García, F., Abati, J., 1997, Variscan accretionary complex of northwest Iberia: Terrane correlation and succession of tectonothermal events. Geology 25, 1103-1106.

Martín-Pozas, J.M., Galán, E., Martín-Vivaldi, J.L. 1971. Il giacimento di caolino di Jove,Lugo, Spagna. I Congresso Nazionale, AIPEA Italia. pp. 89–109.

Middelburg, J.J., Van der Weijden, C.H., Woittiez, J.R.W., 1988. Chemical processes affecting the mobility of major, minor and trace elements during weathering of granitic rocks. Chem. Geol. 68, 253–273.

Murray, H.H. 1988. Kaolin minerals: Their genesis and occurrences. In: Bailey S.W. (Ed.) Hydrous Phyllosilicates (Reviews in Mineralogy, 19), Mineralogical Society of America, Washington, DC, 67-89.

Nesbitt, H.W., 1979. Mobility and fractionation of rare earth elements during weathering of a granodiorite. Nature 279, 206- 210.

Panahi, A., Young, G.M., Rainbird, R.H., 2000. Behaviour of major and trace elements (including REE) during Paleoproterozoic pedogenesis and diagenetic alteration of an Archean granite near Ville Marie, Quebec, Canada. Geochim. Cosmochim. Acta 64, 2199–2220.

Papoulis, D., Tsolis-Katagas, P., Katagas C., 2004. Monazite alteration mechanisms and depletion measurements in kaolins. App. Clay Sci. 24, 271-285.

Pérez-Estaún, A., Bea, F. (Eds.), 2004. Macizo Ibérico. In: Geología de España (J.A. Vera, Ed.) SGE-IGME, Madrid, 19-230.

Putter, T.D., André, L., Bernard, A., Dupuis Ch, Jedwab, J., Nicaise, D., Perruchot, A., 2002. Trace element (Th, U, Pb, REE) 18ehavior in a cryptokarstic halloysite and kaolinite deposit from Southern Belgium: importance of “accessory” mineral formation for radioactive pollutant trapping. App. Geochem. 17, 1313–1328

Schultz, L.G. 1964. Quantitative interpretation of mineralogical composition from X-ray and chemical data for the Pierre shale. U.S. Geological Survey Professional Paper, p. 391C.

Sheppard, S.M.F., Gilg, H.A., 1996. Stable isotope geochemistry of clay minerals. Chem. Geol. 31, 1–24.

Sheppard, S.M.F., Nielsen, R.L., Taylor Jr., H.P., 1969. Hydrogen and oxygen isotope ratios of clay minerals from porphyry copper deposits. Econ. Geol. 66, 515–542.

CAPTIONS OF TABLES AND FIGURES

TABLES

Table 1.- Mineralogical and chemical analysis (major elements in %wt) for the representative rocks of the deposit.

Table 2.- Chemical analysis (trace elements in mg/kg) for the representative rocks of the deposit.

Table 3.- Mineralogical and chemical composition (%wt) for the bulk kaolins.

Table 4.- Mineralogical composition (%wt) of the finer fractions.

Table 5. Chemical composition (major elements in wt%) of the finer fractions.

Table 6. Chemical composition (trace elements in mg/kg) of the bulk samples.

Table 7. Chemical composition (trace elements in mg/kg) of the finer fractions.

Table 8.- H_2O yields, $\delta^{18}O$ and δ D values of the analyzed <1μm size fractions, and $\delta^{18}O$ and δ D average values of the separates with the same sizes.

FIGURES

Figure 1.- Regional geological map of Galicia (NW Spain) after Martinez-Catalán et al. (1997) showing the location of the studied kaolin deposit.

Figure 2.- Panoramic view of the kaolin quarries at Ramón-Fazouro and sketch of the sample location in the studied outcrops.

Figure 3. a) Micro-photographs of felsite (RF-8) showing feldspars crystals in a microcrystalline matrix composed of plagioclase, quartz, muscovite and biotite; b) micaschist (RF-2) showing oriented micaceous minerals bands alternating with quartz plus feldspars bands; c) quartzite (RF-3) (polygonal quartz grains). PXA, 4x.

Figure 4.- a) Halloysite joined to book-like kaolinite aggregate; (b and e)Kaolinite crystals oriented face to face; (c) halloysite crystals in clusters; (d) Halloysite in tubular shape with kaolinite crystals oriented face to face; (f) tubular halloysite crystals and spherical particles which could be allophane.

Figure 5.- a) Major chemical composition normalized to felsite; b) normalized to metapelite.

Figure 6.- a) Trace elements composition normalized to felsite; b) normalized to metapelite.

Figure 7.- a) Felsite normalized REE distribution pattern of the kaolin samples; b) felsite-normalized REE distribution patterns of different grain-size fractions of the same sample.

Figure 8. Cluster analysis.

Figure 9. $\delta^{18}O$ versus δD diagram for the <1 μm fraction of the kaolin. The meteoric water, supergene/hypogene and kaolinite weathering lines (KWL) are given for reference. The dashed line indicates the oxygen and deuterium isotopic composition of water in equilibrium with a kaolinite with the mean isotope ratios ($\delta^{18}O$= 20.4‰ and δD= -74‰). Abundances are expressed as parts per thousand relative to Vienna Standard Mean Ocean Water (V-SMOW).

Figure 10.- Some pictures realized during the visit of Prof. Haydn Murray to Burela kaolin deposit and Sargadelos Ceramic factory (2005) with some of the authors of this paper.

HIGHLIGHTS

New insights on the genesis the largest kaolin deposit in Spain are presented.

Kaolin consists mainly of kaolinite, tubular halloysite, and spherical allophane.

Geochemical analyses of trace and REE show a close relationship between kaolin and associated rocks.

Two kaolin types can be differentiated: (i) massive, associated to felsite; and (ii) related to metapelite

A temperature average of approximately 28ºC was calculated on the basis of the isotopic signatures ($\delta^{18}O$, δD) for the kaolin materials.

Continental weathering was involved in the kaolin formation, but it was not the only process.

These new insights into the genesis of the Burela volcanic-hosted kaolin deposit may provide useful information to guide kaolin regional exploration.

Table

Table 1.- Mineralogical and chemical analysis (major elements in %wt) for the representative rocks of the deposit.

	Felsic volcanic rocks		Altered felsite	Altered metapelite	Quartzite
% wt	RF-5	RF-6	RF-8	RF-2	RF-3
Quartz	24	33	30	27	97
Feldspars	60	67	35	4	
Mica	15		30	31	3
Clay Minerals	Tr	Tr	<5	38	
MIA	29	33	46	87	100
SiO2	73.06	62.33	70.73	65.00	98.86
Al2O3	14.64	20.38	16.21	23.10	0.29
Fe2O3(t)	1.46	1.05	1.06	0.44	0.03
MnO	0.01	<0.01	0.01	<0.01	0
MgO	1.20	0.31	0.56	0.38	0.01
CaO	0.03	0.17	0.09	0.04	0.02
Na2O	2.80	4.93	0.57	0.32	0.02
K2O	5.20	6.49	5.69	3.94	0.12
TiO2	0.19	0.04	0.16	0.90	0.02
P2O5	0.03	0.02	0.03	0.05	0.02
LOI	2.32	3.58	4.92	5.82	0.40
TOTAL	100.94	99.30	100.03	99.99	99.79
CIA	64.58	63.75	71.85	84.31	64.44

Table 2.- Chemical analysis (trace elements in mg/kg) for the representative rocks of the deposit.

	Felsic volcanic rocks		Altered felsite	Altered metapelite	Quartzite
mg/kg	RF-5	RF-6	RF-8	RF-2	RF-3
Sc	0.00	0.00	1.00	12.00	0.00
Be	2.00	1.00	2.00	4.00	0.00
V	0.00	15.41	0.00	79.60	0.00
Cr	0.00	0.00	0.00	106.32	0.00
Ga	20.84	20.30	23.40	28.90	0.00
Ge	1.43	0.00	1.68	0.00	1.14
As	45.17	0.00	26.47	0.00	0.00
Rb	188.80	203.44	240.14	79.49	3.12
Sr	100.39	140.30	55.81	20.07	-4.00
Y	5.91	5.01	43.52	33.02	4.78
Zr	65.72	71.55	76.03	539.03	22.96
Nb	20.40	9.42	26.97	28.91	3.19
Ag	0.00	0.00	0.00	1.15	0.00
Sn	4.67	0.00	4.97	4.62	0.00
Cs	4.35	1.92	11.26	2.39	0.00
Ba	479.43	690.32	140.67	219.77	8.61
W	1.11	0.00	0.00	9.53	0.00
Tl	1.55	1.56	2.25	0.27	0.00
Pb	64.77	43.99	42.54	18.50	0.00
Bi	3.25	1.88	13.67	1.53	0.83
Th	9.25	8.07	10.89	23.38	0.89
U	3.70	2.56	6.11	3.51	0.21
Ta	2.74	2.71	3.41	1.95	0.08
La	24.24	30.92	68.47	85.71	9.89
Ce	35.41	54.11	63.48	159.54	20.41
Pr	3.97	4.04	16.19	16.32	2.04
Nd	14.03	13.83	63.92	57.66	7.24
Sm	3.04	3.02	16.89	10.93	1.30
Eu	0.61	0.56	2.56	1.78	0.24
Gd	2.46	1.83	15.95	7.40	1.27
Tb	0.37	0.28	2.55	1.26	0.21
Dy	1.64	1.15	11.81	6.81	1.13
Ho	0.25	0.16	1.84	1.39	0.20
Er	0.61	0.43	4.85	4.46	0.61
Tm	0.08	0.05	0.67	0.72	0.09
Yb	0.48	0.35	3.76	4.35	0.49
Lu	0.05	0.05	0.47	0.64	0.07
Hf	3.14	3.42	4.03	15.30	1.44

Table 3.- Mineralogical and chemical composition (%wt) for the bulk kaolins.

Samples	RF-1	RF1-05	RF-3-05	RF-5-05	RF-7	RF-12	RF-14	RF-16	RF-17
Quartz	29	30	27	49	36	69	31	22	16
Feldspar	<5	---	<5	28	<5	---	Tr	Tr	---
Kaolin minerals	49	68	56	17	27	22	37	67	74
Mica	17	Tr	13	6	33	9	30	9	9
Others	Sm	Sm	Sm	Sm	Sm	Sm	Sm	Sm	Sm
SiO2	65.36	62.23	58.27	71.12	71.24	91.71	76.31	63.28	59.61
Al2O3	22.68	25.48	27.37	17.2	17.98	5.28	15.17	23.03	27.26
Fe2O3	0.6	0.54	0.54	1.21	0.67	0.07	0.47	0.59	0.56
MnO	0.01	0	0	0.009	0.03	0	0	0.01	0
MgO	0.18	0.07	0.33	0.27	0.36	0.11	0.17	0.13	0.09
CaO	0.04	0.01	0.01	0.03	0.05	0.03	0.05	0.05	0.03
Na2O	0.05	0.03	0.22	0.13	0.16	0.07	0.16	0.07	0.09
K2O	1.82	0.95	3.07	4.84	4.06	0.34	1.37	1.19	0.81
TiO2	0.02	0.02	0.78	0.019	0.02	0.162	0.48	0.02	0.02
P2O5	0.05	0.02	0.04	0.02	0.02	0.03	0.02	0.04	0.02
LOI	8.37	10.02	8.36	5.71	5.5	2.32	5.29	9.17	11.36
TOTAL	99.18	99.37	98.99	100.56	100.09	100.12	99.49	97.58	99.85
CIA	92.23	96.26	89.24	77.48	80.81	92.31	90.57	94.62	96.7

Table 4.- Mineralogical composition (%wt) of the finer fractions.

<45µm						
Sample	Kaolinite	Halloysite	Illite	Quartz	Feldspar	Others
RF-1	37	30	10	16	7	Sm/ All
RF-1-05	45	45	6	Tr	<5	
RF-5-05	56	11	7	24	Tr	
RF-7	41	21	24	12	<5	Sm
RF-14	42	28	12	10	<5	
RF-16	60	15	12	11	Tr	All
RF-17	74	13	<5	8	Tr	Sm/ All
<2µm						
RF-1	54	34	9	Tr		
RF-1-05	58	36	6			
RF-5-05	63	28	9			
RF-7	54	24	15	<5		Sm
RF-14	32	39	<5	26		
RF-16	49	28	<5	17		
RF-17	38	52	Tr	10		
<1µm						
RF-1	25	65		10		
RF-1-05	32	60		8		
RF-5-05	68	26		6		
RF-7	70	20	5			Sm
RF-14	44	37	13	5		
RF-16	30	64		6		
RF-17	23	70		7		

Tr: traces, Sm: smectites, All: Allophane

Table 5. Chemical composition (major elements in wt%) of the finer fractions

Samples	SiO_2	Al_2O_3	Fe_2O_3	MnO	MgO	CaO	Na_2O	K_2O	TiO_2	P_2O_5	LOI	CIA
RF-1-45µm	56.36	29.22	1.02	0.01	0.24	0.05	0.07	2.12	0.02	0.05	10.83	92.88
RF-2 R <45µm	53.67	30.73	0.64	0.003	0.48	0.04	0.32	4.37	1.266	0.06	8.39	86.66
RF-7-45µm	53.92	29.43	1.05	0.02	0.61	0.07	0.11	3.8	0.02	0.02	10.87	88.09
RF-8-45µm	54.25	26.89	2.42	0.013	0.86	0.14	1.24	4.19	0.024	0.07	9.64	82.84
RF-12-45µm	58.92	27.94	0.26	0	0.38	0.06	0.1	1.4	0.41	0.08	10.3	94.71
RF-14-45µm	49.98	32.21	1.13	0	0.37	0.05	0.17	2.2	1.19	0.04	12.14	93.01
RF-16-45µm	47.03	31.5	0.74	0.01	0.16	0.04	0.07	1.45	0.02	0.05	18.98	95.28
RF-17-45µm	48.42	35.5	0.66	0	0.1	0.04	0.08	1.02	0.02	0.01	14.18	96.89
RF-16<2µm	49.99	33.4	0.85	0.01	0.12	0.09	0.06	1.26	0.02	0.05	13.13	95.95
RF-17<2µm	44.77	36.93	0.4	0	0.05	0.1	0.04	0.1	0.01	0.02	16.79	99.35

Table 6. Chemical composition (trace elements in mg/kg) of the bulk samples.

	RF-1	RF-1-05	RF-3-05	RF-5-05	RF-7	RF-12	RF-14	RF-16	RF-17
Rb	105	59	63	213	164	10	24	84	63
Sr	23	8	25	41	31	6	12	21	4
Ba	50	20	31	119	171	12	125	47	10
Cs	6	6	1	10	6	1	1	7	5
Zr	106	77	223	71	85	300	277	106	68
Hf	5	4	6	4	4	9	8	5	4
Ta	4	3	1	3	4	0	1	4	3
Nb	34	22	19	25	26	8	17	32	20
U	4	2	3	3	3	1	2	2	2
Th	15	14	23	12	12	5	12	16	11
Cr	0	20	90	0	0	0	43	0	0
Pb	52	75	19	3	66	0	0	53	13
Y	31	41	21	16	24	7	13	11	3
Sc	4	5	12	3	3	2	6	3	4
La	36	34	34	12	26	29	29	40	9
Ce	82	51	74	23	46	56	55	70	11
Pr	10	5	7	3	6	6	6	7	1
Nd	42	14	24	13	23	20	20	25	3
Sm	10	3	5	3	6	3	4	5	1
Eu	2	0	1	1	1	1	1	1	0
Gd	9	2	3	3	8	2	3	4	1
Tb	2	0	1	1	1	0	1	1	0
Dy	8	1	3	3	6	2	3	3	1
Ho	1	0	1	0	1	0	1	0	0
Er	3	0	2	1	3	1	2	1	0
Tm	0	0	0	0	0	0	0	0	0
Yb	3	0	2	1	2	1	2	1	0
Lu	0	0	0	0	0	0	0	0	0
∑REE	209	110	157	65	129	122	124	159	29
∑HREE	191	108	147	58	116	117	116	152	27
∑LREE	49	43	31	22	37	12	22	17	5
Eu/Eu*	3	1	1	1	2	1	1	1	0
La/Yb	13	101	14	11	13	27	16	39	24
La/Sm	4	14	7	4	4	9	7	8	10
Gd/Yb	3	5	1	3	4	2	2	4	2
Th/U	4	8	9	4	4	6	6	7	6
La/Th	2	3	2	1	2	5	2	2	1
Sm/Nd	0	0	0	0	0	0	0	0	0

Table 7. Chemical composition (trace elements in mg/kg) of the finer fractions.

	RF-1 <45	RF-7<45	RF-8<45	RF-12<45	RF-14<45	RF-16 <45	RF-17<45	RF-16 <2	RF-17 <2
Rb	129	189	185	32	54	105	75	92	13
Sr	28	23	32	30	15	28	6	34	21
Ba	47	99	72	41	213	63	14	70	25
Cs	7	9	12	3	2	9	7	8	2
Zr	137	172	146	368	605	126	94	142	83
Hf	7	8	8	11	18	6	5	7	4
Ta	6	7	6	1	3	5	4	6	4
Nb	45	44	46	13	46	42	25	39	22
U	5	6	16	2	6	3	2	4	5
Th	20	24	21	19	36	21	13	27	21
Cr	44	0	82	83	332	0	0	30	50
Pb	49	59	28	0	21	57	18	76	43
Y	42	52	77	20	34	14	4	22	6
Sc	8	4	3	12	12	7	4	6	2
La	51	52	108	100	93	54	12	52	30
Ce	116	73	107	192	178	94	15	100	36
Pr	13	11	26	19	18	9	1	10	3
Nd	59	45	100	66	64	32	4	35	9
Sm	15	12	27	11	11	7	1	7	2
Eu	2	2	4	2	2	1	0	1	0
Gd	13	13	25	7	8	5	1	6	2
Tb	2	2	4	1	1	1	0	1	0
Dy	10	11	20	5	7	4	1	5	2
Ho	2	2	3	1	1	1	0	1	0
Er	5	5	8	3	5	2	1	2	1
Tm	1	1	1	0	1	0	0	0	0
Yb	4	4	6	3	5	1	0	2	1
Lu	0	1	1	0	1	0	0	0	0
∑REE	293	235	440	410	396	211	37	222	85
∑HREE	269	209	397	397	374	203	34	212	82
∑LREE	66	78	120	33	56	22	7	32	10
Eu/Eu*	4	3	7	3	3	2	0	2	0
La/Yb	14	12	17	40	18	43	25	33	60
La/Sm	3	4	4	9	8	8	12	7	15
Gd/Yb	4	3	4	3	2	4	2	4	3
Th/U	4	4	1	10	6	7	6	7	4
La/Th	2	2	5	5	3	3	1	2	1
Sm/Nd	0	0	0	0	0	0	0	0	0

Table 8.- H_2O yields, $\delta^{18}O$ and δ D values of the analyzed <1μm size fractions, and $\delta^{18}O$ and δ D average values of the separates with the same sizes.

Sample	H_2O (%)	$\delta^{18}O$ (‰)	δD (‰)
RF-1	7.3	20.2	-69
RF-7	6.8	20.8	-85
RF-14	7.1	20.2	-84
RF-16	7.7	20.7	-68
RF-17	7.3	20.2	-63
RF-1-05	8.0	21.0	-79
RF-5-05	7.5	19.8	-71
Mean	7.4	20.4	-74

Figure
Click here to download Figure: FIGURES BURELA MS 15_11_17.docx

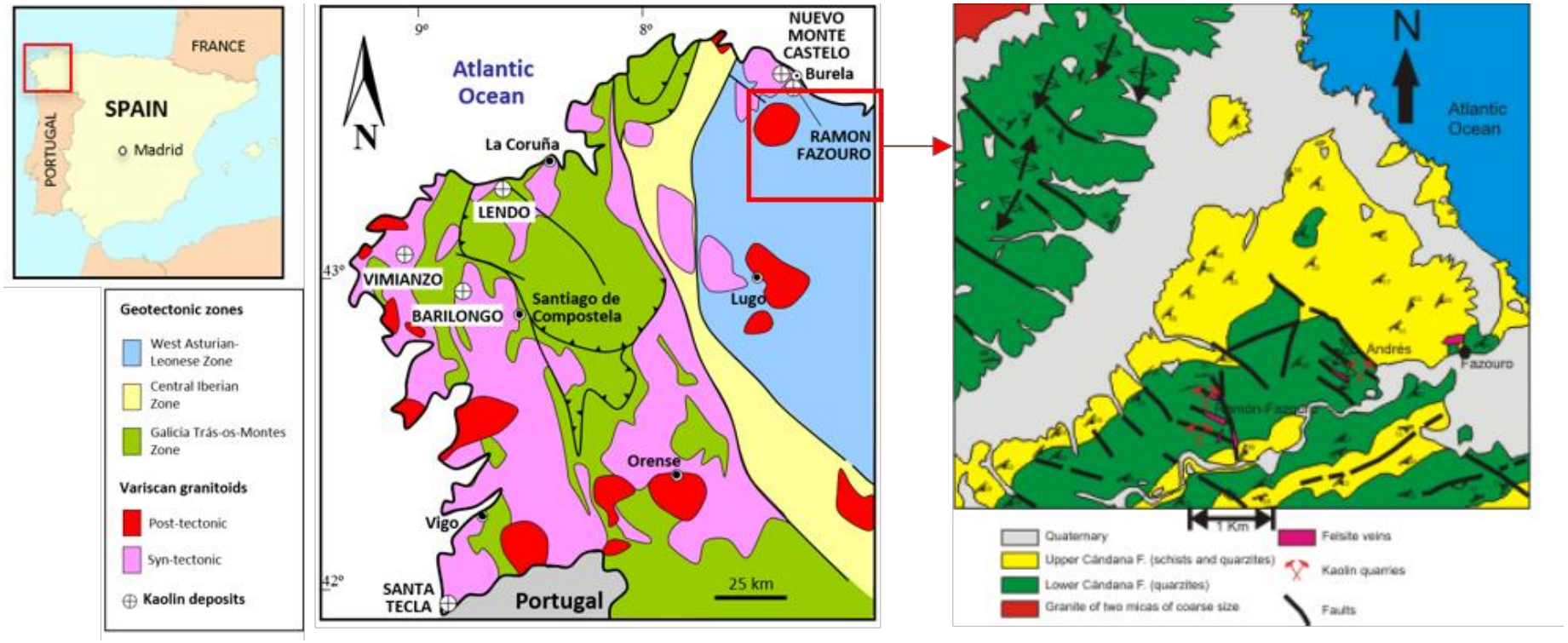

Figure 1.- Regional geological map of Galicia (NW Spain) after Martinez-Catalán et al. (1997) showing the location of the studied kaolin deposit.

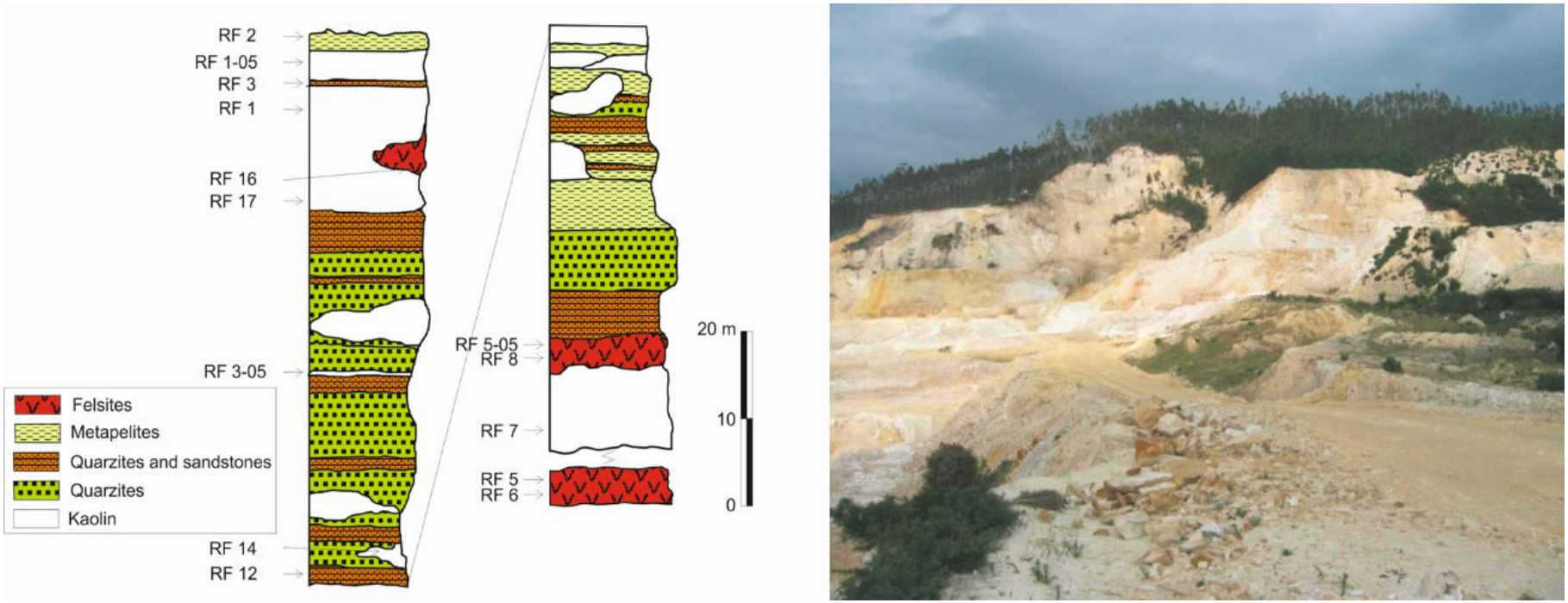

Figure 2.- Panoramic view of the kaolin quarries at Ramón-Fazouro and sketch of the sample location in the studied outcrops.

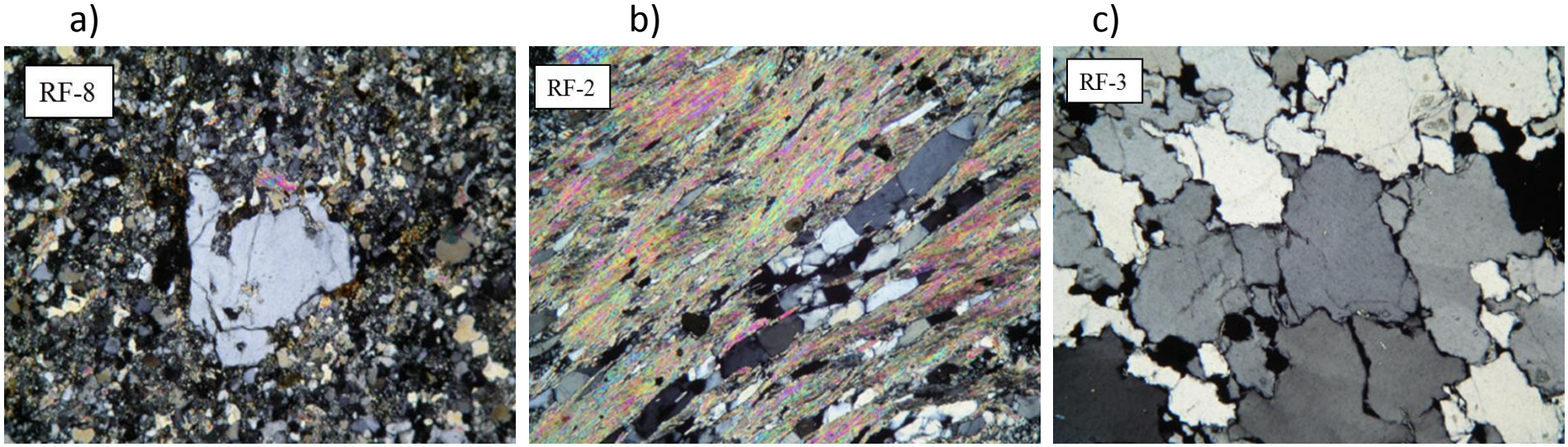

Figure 3. a) Micro-photographs of felsite (RF-8) showing feldspars crystals in a microcrystalline matrix composed of plagioclase, quartz, muscovite and biotite; b) micaschist (RF-2) showing oriented micaceous minerals bands alternating with quartz plus feldspars bands; c) quartzite (RF-3) (polygonal quartz grains). PXA, 4x.

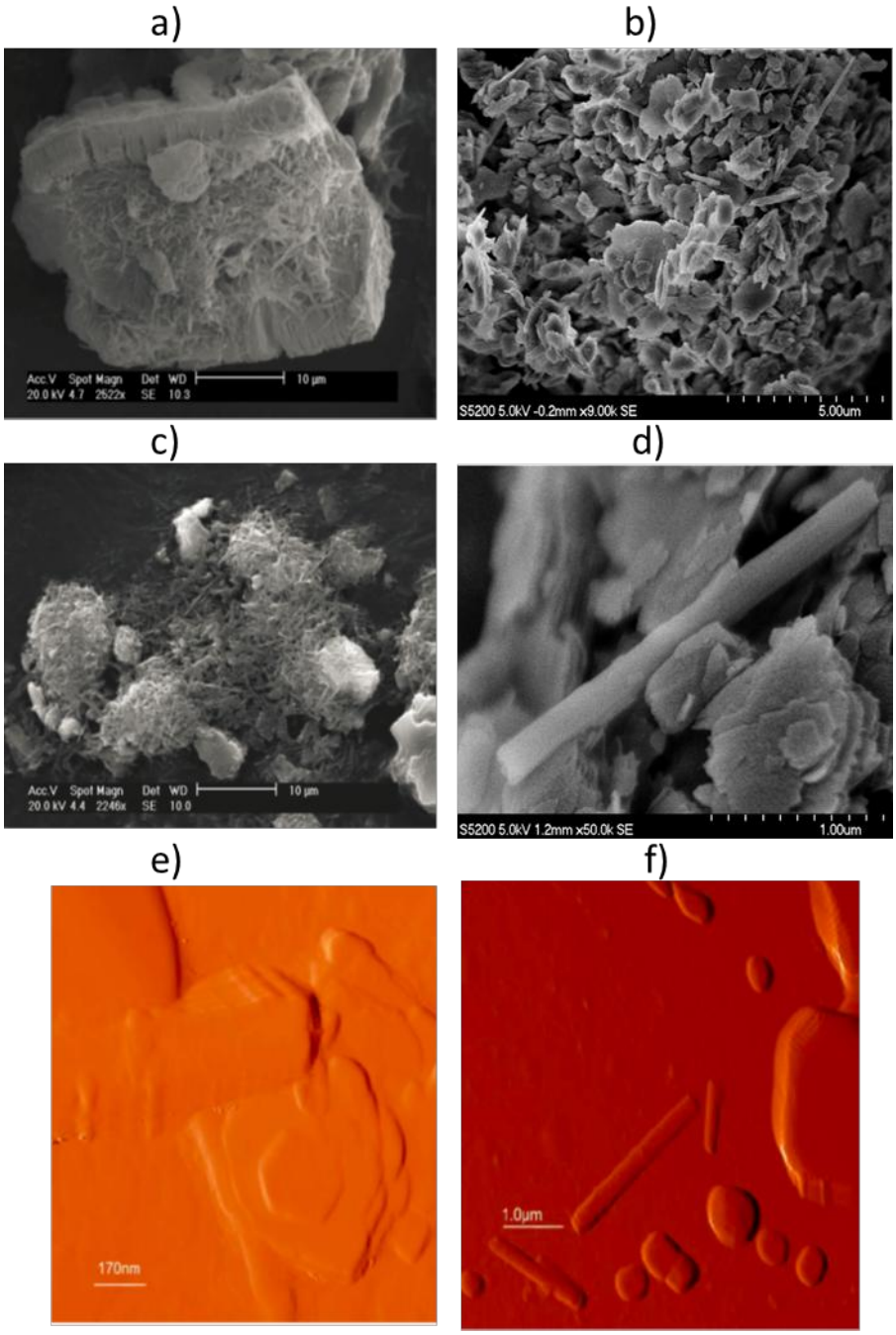

Figure 4.- a) Halloysite joined to book-like kaolinite aggregate; (b and e)Kaolinite crystals oriented face to face; (c) halloysite crystals in clusters; (d) Halloysite in tubular shape with kaolinite crystals oriented face to face; (f) tubular halloysite crystals and spherical particles which could be allophane.

a)

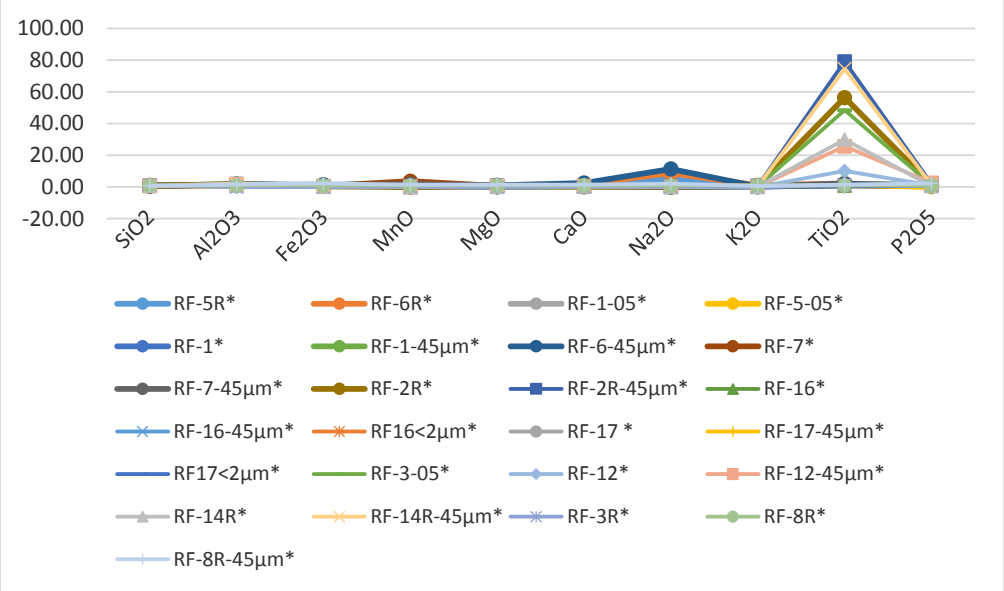

b)

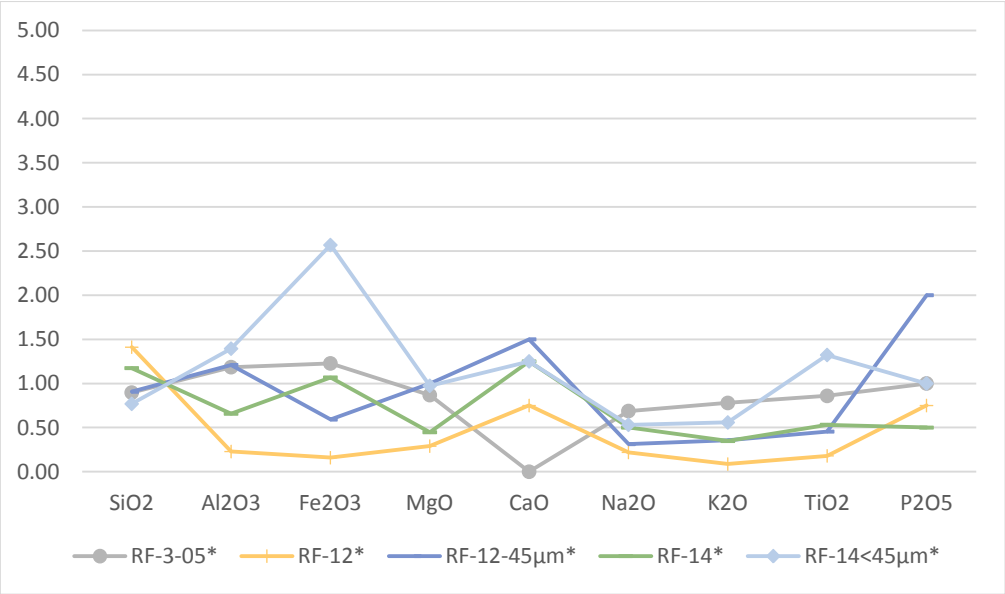

Figure 5.- a) Major chemical composition normalized to felsite; b) normalized to metapelite.

a)

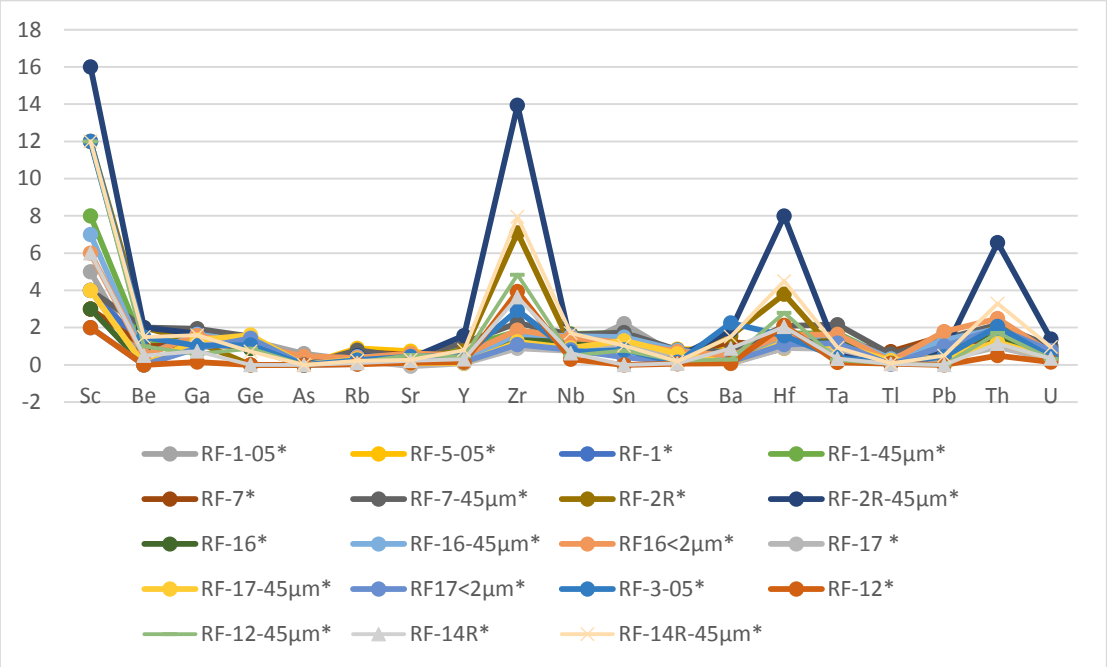

b)

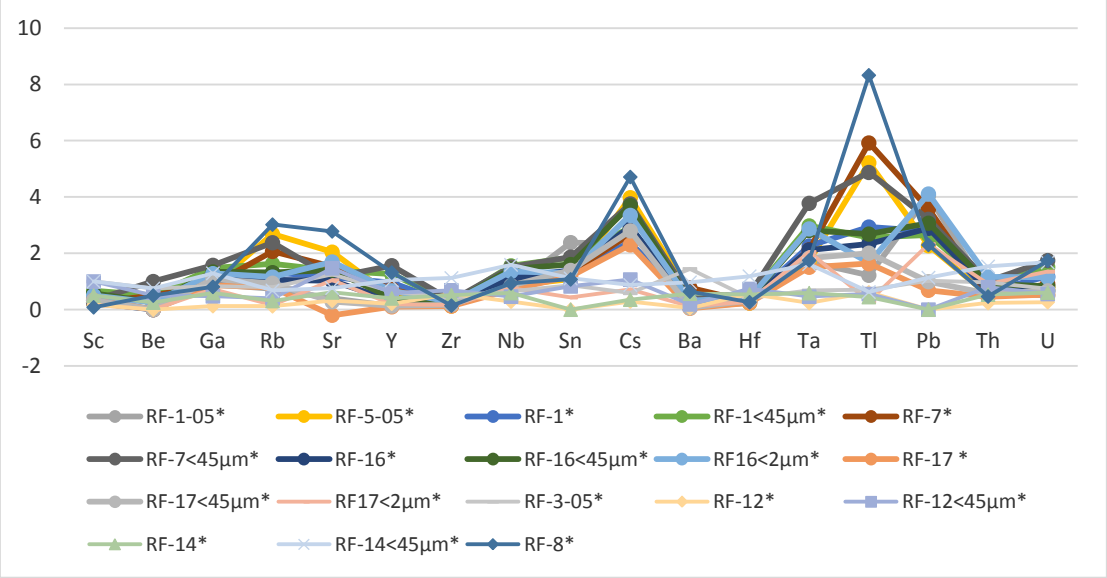

Figure 6.- a) Trace elements composition normalized to felsite; b) normalized to metapelite.

a)

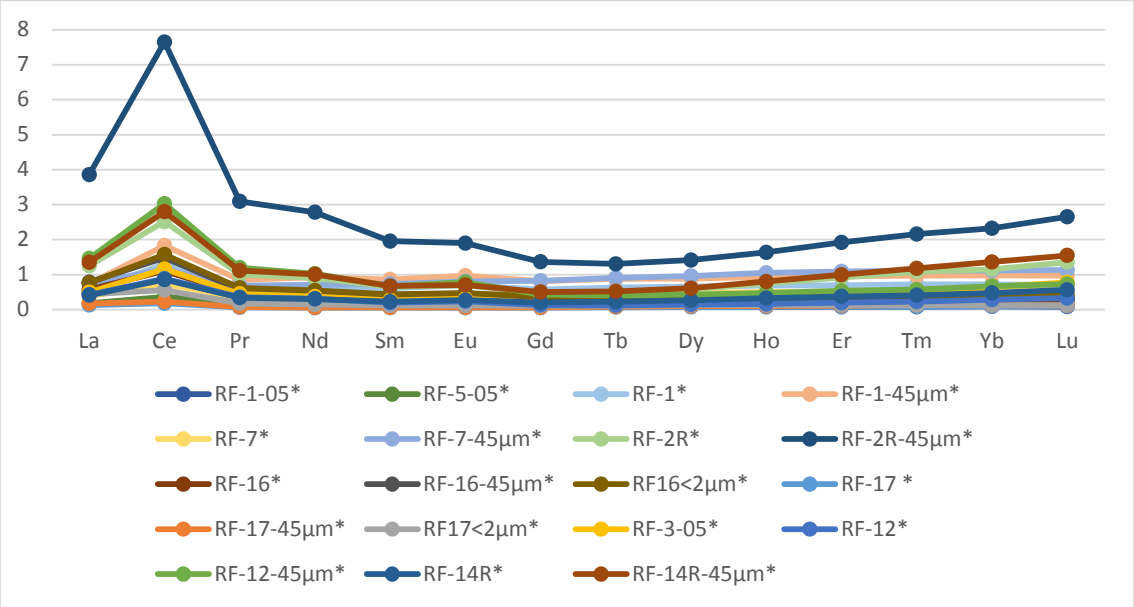

b)

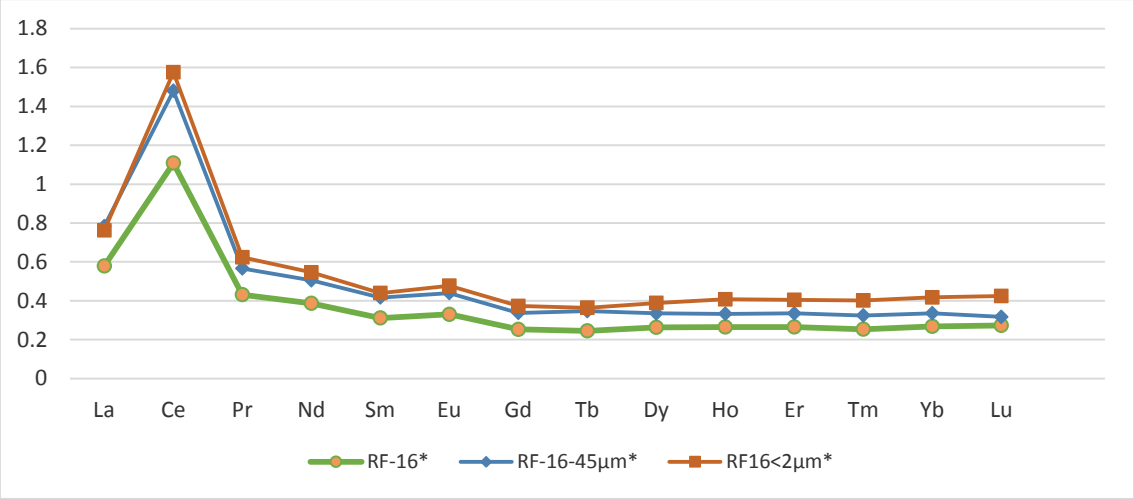

Figure 7.- a) Felsite normalized REE distribution pattern of the kaolin samples; b) felsite-normalized REE distribution patterns of different grain-size fractions of the same sample.

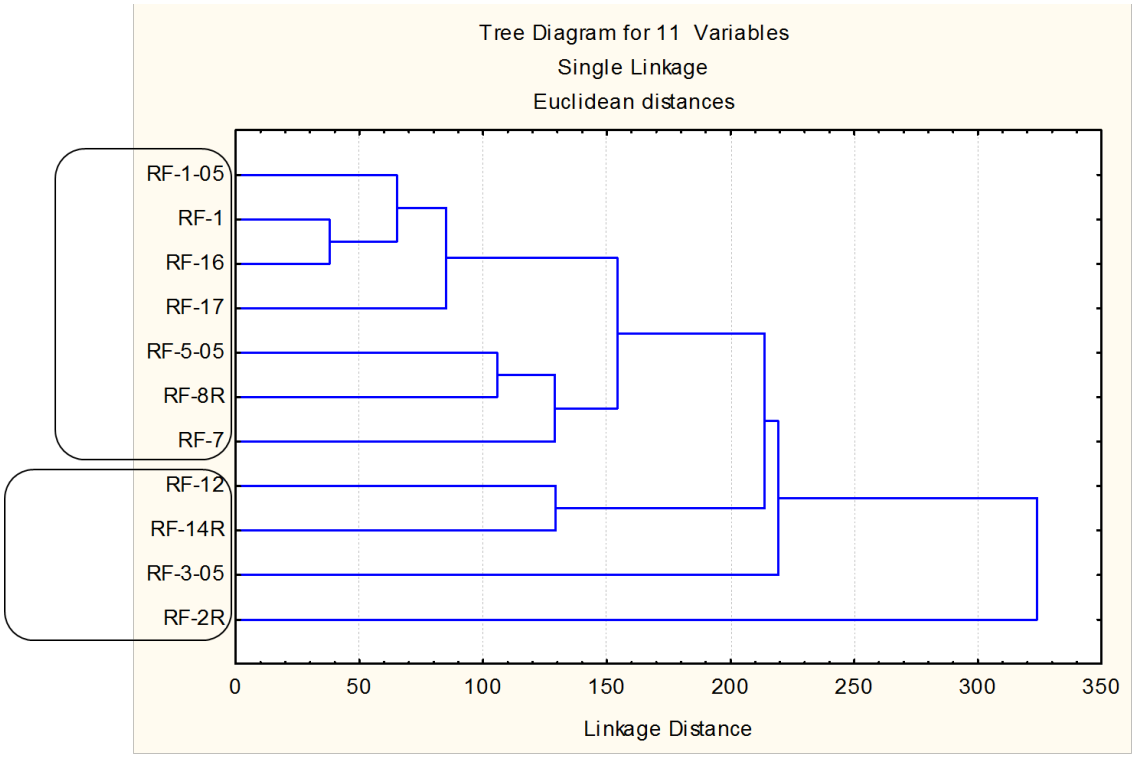

Figure 8. Cluster analysis

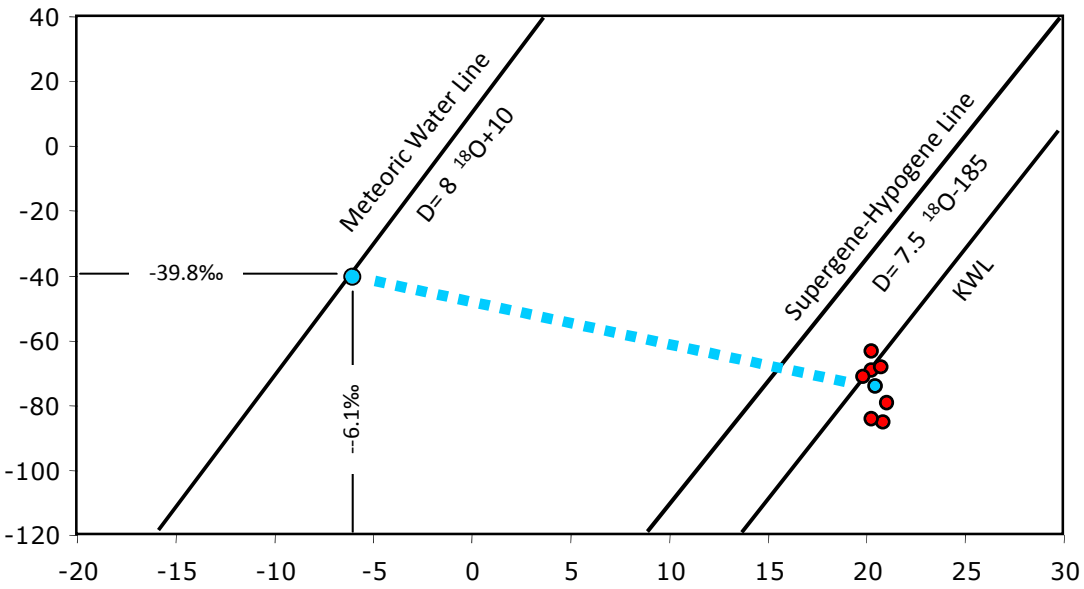

Figure 9. $\delta^{18}O$ versus δD diagram for the <1 μm fraction of the kaolin. The meteoric water, supergene/hypogene and kaolinite weathering lines (KWL) are given for reference. The dashed line indicates the oxygen and deuterium isotopic composition of water in equilibrium with a kaolinite with the mean isotope ratios ($\delta^{18}O$= 20.4‰ and δD= -74‰). Abundances are expressed as parts per thousand relative to Vienna Standard Mean Ocean Water (V-SMOW).

Figure 10.- Some pictures realized during the visit of Prof. Haydn Murray to Burela kaolin deposit and Sargadelos Ceramic factory (2005) with some of the authors of this paper.

NEW INSIGHTS ON MINERALOGY AND GENESIS OF KAOLIN DEPOSITS: THE BURELA KAOLIN DEPOSIT (NORTHWESTERN SPAIN)

ABSTRACT

The Burela deposit is the largest kaolin deposit in Spain, mined for more than 50 years, the product being mainly used for porcelain. Kaolin is dominantly associated with Lower Cambrian felsites, interbedded with quartzites, micaschists and metapelites (Cándana Series), and was strongly folded during the Hercycian orogeny. Kaolin layers were ductile and incompetent materials among more competent ones, producing many slides with a diastrophic appearance. Consequently, kaolin outcrops are morphologically very variable, -i.e. pockets -, and interlayered between metapelites and/or quartzites, resulting in complication for prospection and mining.

The kaolin consists mainly of kaolinite, tubular halloysite, and spherical allophane along with quartz and minor illite. The content of kaolin minerals reaches up to 90% in the finer fraction (<2μm and <1μm).

Geochemical analyses of trace and REE show a close relationship between kaolin and associated rocks. Two kaolin types can be differentiated: (i) massive, associated to felsite; and (ii) related to metapelite. A temperature range from 20 to 35°C, with an average of approximately 28ºC was calculated on the basis of the isotopic signatures ($\delta^{18}O$, δ D) for the kaolin materials. This scatter suggests that if continental weathering was involved in the kaolin formation on the lower side of the temperatures, it was not the only process, especially for kaolin associate with felsites and metapelites. The higher temperatures are indicative of a hydrothermal auto-metamorphic alteration, followed by a folding of the series that induced an apparently chaotic kaolin distribution with a combined continental weathering superimposed on the previous low-temperature hydrothermal felsite transformation.